RSC Advances

PAPER

View Article Online
View Journal | View Issue

Cite this: *RSC Adv.*, 2020, **10**, 18259

Synthesis and characterisation of novel Cu(II)-anchored biopolymer complexes as reusable materials for the photocatalytic degradation of methylene blue

Murugaiyan Manimohan,[a] Sivashanmugam Pugalmani,[b] K. Ravichandran[c] and Mohamed Aboobucker Sithique *[a]

This study focused on the synthesis, photocatalytic degradation of organic dyes and biological activity of novel N, N, O-donor tridentate water soluble 4-hydroxy benzohydrazide-grafted biopolymer Schiff base Cu(II) complexes. The eco-friendly catalysts were designed for potential application in the degradation of organic dyes. The photocatalytic degradation of methylene blue was investigated with various irradiation times (30, 60, 90 and 120 min), catalytic dosages (5, 10, 15 and 20 mg) and pH (3, 7 and 12). The as-prepared compounds were characterised *via* various techniques including FT-IR and FT-NMR spectroscopy; TGA-DTA, XRD, SEM-EDAX; ESR and UV-vis spectroscopy; photoluminescence, magnetic moment, and conductivity measurements; and elemental and thermal analysis. The crystallinity of the Schiff base ligands, chitosan, and their Cu(II) complexes was analysed *via* X-ray diffraction (XRD) studies. The XRD patterns revealed that the polymer chitosan was more crystalline than the Schiff base ligands and their complexes. The surface morphological analysis by scanning electron microscopy (SEM) revealed that the Cu(II) complexes were amorphous in nature compared to chitosan and the ligands. The anti-inflammatory and anti-diabetic studies of the biopolymer Cu(II) complexes were performed using the albumin denaturation technique and McCue and Shetty method, respectively. The as-synthesized 4-hydroxy benzohydrazide-grafted *O*-carboxymethyl chitosan Schiff base ligands and their Cu(II) complexes showed a good anti-inflammatory and antidiabetic effect. The photocatalytic activity proved that the aryl-substituted complex was more efficient than the aliphatic-substituted complex.

Received 22nd February 2020
Accepted 6th April 2020

DOI: 10.1039/d0ra01724h

rsc.li/rsc-advances

1. Introduction

Untreated dyes from industrial effluent cause severe damage to the environment, resulting in a decline in biodiversity in the aquatic ecosystem. Besides, they also lead to water pollution and desertification. Therefore, dye-containing hazardous substances need to be treated before their disposal. Consequently, many physicochemical techniques such as precipitation, filtration, coagulation or flocculation, flotation, adsorption, oxidation, chlorination, bleaching, ozonation, Fenton oxidation, ion exchange, reverse osmosis and biological techniques including aerobic and anaerobic processes are utilized for the treatment of industrial effluent. However, these techniques often exhibit a low removal efficiency and involve high capital costs in the dye removal process.[1,2] On the other hand, biopolymer metal complexes as photocatalysts function more efficiently towards dye degradation, often resulting in the complete elimination of hazardous substances from the environment.[3]

Chitosan has found diverse applications due to its physicochemical properties. It is widely employed in several areas such as the biological, pharmaceutical, biomedical, and industrial fields.[4–6] Furthermore, several chemical modification techniques are available to enhance its physical and chemical properties. These techniques include carboxymethylation, Schiff base formation, sulfonation, phosphorylation, quaternization, formylation, acylation, carboxylation, enzymatic substitution, metal chelation, nitration and cyanoethylation.[7] The carboxymethylation process of chitosan makes the polymer often advantageous because it uses low cost catalysts and the resulting product is eco-friendly, water soluble, non-toxic, moisture absorbent, hydrophobic and biodegradable with metal affinity, and medicinal and industrial applications.[8]

4-Hydroxy benzohydrazide-grafted biopolymer Schiff base ligands consisting (azomethine-N donor, pyridyl-N donor and enolate-O donor atoms) of enriched π electrons have affinity for

[a]*PG & Research Department of Chemistry, Islamiah College (Autonomous), Vaniyambadi, Tirupattur District, Tamil Nadu– 635 752, India. E-mail: masithique@gmail.com*

[b]*State Key Laboratory of Tribology, Tsinghua University, Beijing, China*

[c]*Department of Analytical Chemistry, University of Madras, Guindy Campus, Chennai, India*

metal ions.[9] This property (complexation/chelation/coordination) is beneficial for the formation of transition metal complexes, which have applications in several chemical, photochemical and photobiological degradation processes.[10,11] Recently, an increasing number of these metal complexes have been employed in the degradation of organic dyes and removal of organic pollutants such as CO_2 and H_2O.[12–14]

The azo dye methylene blue (MB) is acidic (pH = 3) in nature, which strongly adheres in the interstitial spaces of cotton fibres and firmly fixed on fabric in the textile industry.[15,16] Recent studies have reported several biopolymer photocatalysts for the organic dye removal process. Methylene blue degradation also has been investigated, and various forms of biopolymer nano-photocatalysts such as ZnO nanoflowers,[17] cellulose nanocrystals,[18] chitosan nanocomposite,[19,20] cellulose microfibers,[21] chitosan microspheres,[22] nanoparticles,[23,24] nanosheets,[25] multi-walled nanotubes,[26] nanomaterials,[27] nanostructure compounds[28–30] and various forms of metal complexes such as trinuclear complexes,[31] binuclear complexes,[32] one-dimensional complexes,[33] and multifunctional complexes[34] have been effectively used in the degradation of dyes. However, there has hardly been any report on the application of biopolymer Schiff base complexes in the photocatalytic degradation of dyes.

In the present study, biopolymer *O*-carboxymethyl chitosan Schiff base Cu(II) complexes were synthesized. The method adopted gave a high yield and the prepared complexes were proven to be very cheap photocatalysts for the dye removal process. The prepared sustainable catalysts have the advantages of biocompatibility, photodegradability, low-cost, stability, eco-friendliness, easy accessibility and reusability. The biopolymer/*O*-CMCS Schiff base Cu(II) complexes were used as novel photocatalysts for the degradation of methylene blue dye. Furthermore, various factors such as catalyst dosage, irradiation time and the pH were optimised, which resulted in better dye degradation than the reported studies. In additional to the synthesized copper(II) complexes being novel, their anti-inflammatory (egg albumin denaturation) and antidiabetic nature are also novel.

2. Results and discussion

The biopolymer Schiff base ligands (SB_1 and SB_2) were fully soluble in water, and their metal complexes [(SB_1)–Cu($OAc)_2$] and [(SB_2)–Cu($OAc)_2$], respectively, were soluble in *N*,*N*-dimethylformamide, dimethylsulphoxide and hot water, but insoluble in methanol, ethanol and chloroform,[35] as shown in Table 1.

2.1 Elemental analysis

Elemental analysis was carried out to determine the presence of various elements in DCS, SB_1, SB_2, and their Cu(II) complexes. Subsequently, the percentage ratio of constituents (C, H and N) in the compounds was theoretically calculated for the deacetylated chitosan (DCS), Schiff bases (SB_1 and SB_2) and their Cu(II) metal complexes. The theoretically calculated and experimentally obtained values were both almost the same. The degree of deacetylation (DD) of chitosan was calculated using the following formula:

$$\text{Degree of deacetylation} = 1 - \left[\frac{\left(\frac{C}{N} - 5.145\right)}{1.536}\right] \times 100 \quad (1)$$

where C/N is the ratio of carbon to nitrogen. The degree of substitution (DS) of the hydrazide-based ligands SB_1 and SB_2 was calculated using the formula

$$\text{Degree of substitution} = \frac{\left(\frac{aC}{N}\right)s - \left(\frac{C}{N}\right)i}{n} \quad (2)$$

where *a* is the number of nitrogen atoms and *n* is the number of carbon atoms after modification of the chitosan Schiff base. (C/N)s is substituted chitosan through Schiff base formation and (C/N)i the unsubstituted initial chitosan. The degree of substitution (DS) of the biopolymer Schiff base ligands SB_1 and SB_2 was 0.46 and 0.48, respectively,[36] as shown in Table 2.

2.2 FT-IR studies

Chitosan (CS) (Fig. 1a), deacetylated (~97%) chitosan (DCS) (Fig. 1b), ligands SB_1 and SB_2 (Fig. 1c and d) and Cu(II) complexes of SB_1 and SB_2 (Fig. 1e and f) were characterised by FT-IR spectroscopy, respectively. A broad band appeared around 3400 cm^{-1} for CS, which can be ascribed to the –OH stretching, symmetric and asymmetric stretching of $-NH_2$ and intermolecular hydrogen bonding. Another broad band appeared at 2908 cm^{-1}, which can be attributed to the presence of ($-CH_2$) groups in the pyranose ring. The peaks at 1655 cm^{-1} and 1600 cm^{-1} are attributed to the carbonyl (C=O stretching) group and amine ($-NH_2$ bending) group of the amide (–NH–CO–CH_3), respectively. The peaks at 1082 cm^{-1} and 1032 cm^{-1} correspond to the (–C–O)

Table 1 Yield and solubility of DCS, as-synthesized 4-hydroxy benzohydrazide-based biopolymer/*O*-carboxymethyl chitosan Schiff bases and their Cu(II) complexes

Name of the compound/ligand/complex	Soluble in (solvent)	Reactant (g)	Yield (g)	Yield (%)
Deacetylated chitosan (DCS)	Mineral and organic acids	5	4.864	97.28
(SB_1)	Water	2.16	1.64	75.92
(SB_2)	Water	2.18	1.62	74.77
[(SB_1)–Cu($OAc)_2$]	DMSO, DMF	0.80	0.43	53.75
[(SB_2)–Cu($OAc)_2$]	DMSO, DMF	0.80	0.46	57.50

Table 2 Elemental analysis data of percentage of C, H and N in 4-hydroxy benzohydrazide-based *O*-carboxymethyl chitosan Schiff base and their Cu(II) complexes

Name of the compound/Schiff base ligands/complexes	Theoretically calculated (%)				Actually found (%)			
	C	H	N	C/N	C	H	N	C/N
DCS	44.44	7.40	8.64	5.14	43.56	6.38	8.40	5.19
(SB_1)	55.02	5.96	9.63	5.71	55.08	6.03	9.47	5.82
(SB_2)	64.26	5.36	7.50	8.57	63.86	5.48	7.61	8.39
[(SB_1)–$Cu(OAc)_2$]	46.59	5.18	6.80	6.85	47.27	5.62	6.96	6.79
[(SB_2)–$Cu(OAc)_2$]	54.96	4.85	5.66	9.71	55.19	4.39	5.71	9.66

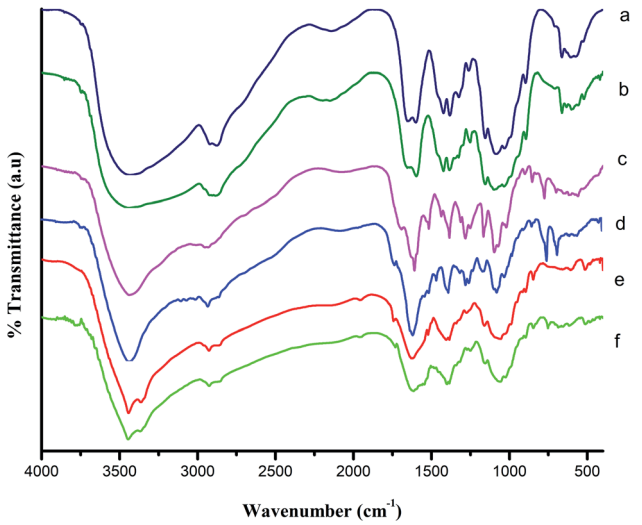

Fig. 1 Fourier transform infrared spectra of (a) 90% deacetylated chitosan (CS), (b) DCS, (c) SB_1, (d) SB_2, (e) SB_1–$Cu(OAc)_2$, and (f) SB_2–$Cu(OAc)_2$.

asymmetric stretching and –C–O stretching of the primary alcoholic group, respectively. Broad bands were observed for DCS in the region of 3436 cm^{-1} due to the secondary amine (–NH) and –OH groups and 2905 cm^{-1} for the $-CH_2$ symmetric stretching. The peak at 1655 cm^{-1} corresponds to the carbonyl group of the amide (NH–CO–CH_3), which shifted to 1596 cm^{-1} after the deacetylation of CS, confirming the formation of free NH_2 groups in DCS.[37,38]

The FTIR spectra of the ligands (SB_1 and SB_2) showed the disappearance of the peak at 1596 cm^{-1} ($-NH_2$ bending vibration of DCS) and the appearance of peaks for the Schiff base ligand SB_1 at 1609 cm^{-1} and Schiff base ligand SB_2 at 1613 cm^{-1} (–C=O), demonstrating the chemical modification of DCS. The Schiff base ligands showed sharp signals at 1517 cm^{-1} and 1510 cm^{-1}, corresponding to the azomethine group (–CH=N–) stretching vibrations. These observed signals indicate the condensation reaction of the Schiff base ligand (precursor) with DCS. Strong absorption bands were observed at 1385 cm^{-1} and 1097 cm^{-1} for SB_1 and 1385 cm^{-1} and 1074 cm^{-1} for SB_2. These bands in both SB_1 and SB_2 confirm the presence of C–N axial deformation of amino groups and hydrazone coupling (>C=N–NH) stretching frequencies, respectively. The band at 1032 cm^{-1} in the spectrum of (–C–O stretching of primary alcoholic group) CS disappeared and appeared at 1692 cm^{-1} for SB_1 and 1730 cm^{-1} for SB_2, respectively. This demonstrated the formation of a carboxymethyl group at C_6–OH of the chitosan pyranose ring.[39]

After the complexation, the carbonyl (C=O) group stretching vibrations of ligands SB_1 and SB_2 shifted to a higher wavenumber by 1 to 25 cm^{-1} due to the involvement of the imine group (>C=N) nitrogen atom in coordination with the metal ion (π–π conjugate). Further, the coordination between the metal ion and Schiff base ligands (SB_1 and SB_2) *via* the donor oxygen of the carbonyl group (M–O) appeared at 515 cm^{-1} and 513 cm^{-1}, respectively.[40] Similarly, the new peaks that appeared at 419 cm^{-1} and 420 cm^{-1} are attributed to the (M–N) stretching vibration. Additionally, the π–π conjugation between the copper metal ion and acetate carbonyl group was observed at 1407 cm^{-1} and 1385 cm^{-1} for the Cu(II) complexes of SB_1 and SB_2, respectively. After the complexation, the hydrazone group of the (>C=N–NH–) amido form was retained from the azine (=N–N=) form in the spectra of the Cu(II) complexes of the biopolymer Schiff base ligands.[41,42]

2.3 ^1H and ^{13}C NMR

The ^1H and ^{13}C NMR spectra of compounds SB_1 and SB_2 were analysed and shown in Fig. 2a and b. The ^1H NMR spectrum of Schiff base ligand SB_1 showed peaks at the chemical shift (δ) values of 1.95 3H(s), 3.06 3H(s) and 3.63 3H(s) due to the presence of methyl group protons. The peak at δ 3.80 2H(s) indicates the presence of methylene ($-CH_2$) group protons. The sharp signal at δ 6.19 reveals the presence of imine C=NH(s) protons. This confirmed the formation of the Schiff base (SB_1) ligand. The signals at δ 7.45 H(d), 7.59 H(d), and 7.91 H(s) indicate the presence of aromatic protons. The signal at δ 10.66 confirms the presence of a hydrazide secondary amine (O=C–NH–) group. The signal at δ 14.41 indicates the acidic (–COOH) proton. This confirms the presence of the carboxymethyl group in the polymer.[43]

The ^{13}C NMR spectrum of the hydrazide-grafted Schiff base ligand SB_1 showed a peak at a chemical shift (δ) value of 192.85 ppm, which confirms the presence of the carboxylic acid group of carboxymethyl chitosan. The strong signals located at δ 178.51 and 177.21 confirm the presence of the imine linkage (–C=N) and hydrazide (–CO–NH–) linkage carbon atoms, respectively. The signals at 128, 129.69, 133.3 and 135.7 ppm indicate the presence of aromatic carbon atoms and the peak at

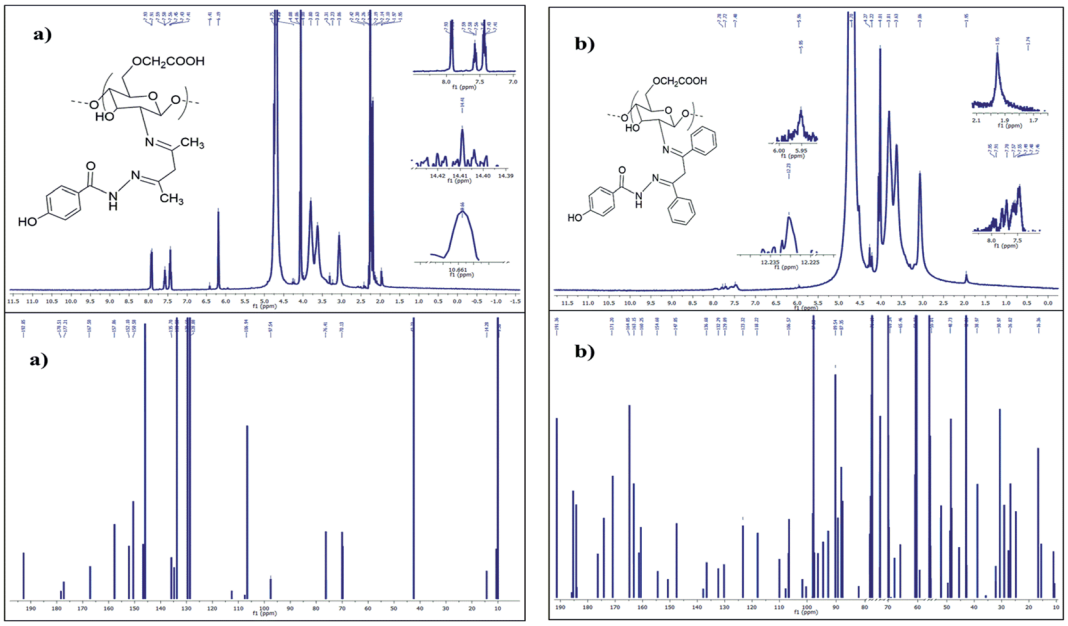

Fig. 2 (a) ^{1}H and ^{13}C Fourier transform-nuclear magnetic resonance spectra of SB_1. (b) ^{1}H and ^{13}C Fourier transform-nuclear magnetic resonance spectra of SB_2.

δ 42.73 indicates the methylene (–CH_2) carbon atom of β-diketone.[44]

Similarly for SB_2, its ^{1}H NMR spectrum showed a signal at δ 3.81 2H(s), which represents the methylene group protons. The peak at δ 5.96 NH(s) is attributed to the imine proton. The signals at δ 7.48 H(d), 7.72 H(d), and 7.78 H(s) indicate the presence of aromatic protons in SB_2. The peak at δ 12.23 H(s) corresponds to the carboxymethyl proton.

The ^{13}C NMR spectrum of the SB_2 ligand was examined, and peaks were observed at δ 191.36 for the carboxymethyl group, and δ 171.20 and 164.85 for the imine (C=N) carbon atom and hydrazide carbon atom (–CO–NH–) of SB_2, respectively. This confirmed the formation the biopolymer/*O*-CMCS Schiff base ligand. The peaks that appeared at δ 147.85, 136.68, 132.29, 129.89, 123.32 and 118.22 are due to the aromatic carbon atoms. The peak at δ 42.86 represents the methylene carbon atom.[45]

2.4 Ultraviolet-visible analysis

It has been reported that no transitions are observed between 300 and 800 nm in the electronic spectrum of fully deacetylated chitosan (DCS).[46] The UV-vis spectra of the synthesized Schiff bases showed absorptions at 261.56 nm and 305.33 nm for 3a-OCMCS and 266.73 nm and 306.86 nm for 3b-OCMCS. These absorption peaks are attributed to the π–π* transition for the aromatic ring (C=C) and n–π* transition for the Schiff base imine (–C=NH), respectively. The π–π* transition indicates the presence of an aromatic double bond in the Schiff base ligands and the n–π* transition reveals the formation of an imine group in which the hetero atom nitrogen is coordinated with an alkene carbon atom. Following the complexation, the π–π* and n–π* transitions of the complexes shifted to higher wavelengths of ~380 and ~490 nm, respectively, due to the involvement of the oxygen and nitrogen atoms of the ligand in the coordination. Also, the weak d–d transitions of the complexes appeared close to 780 nm, which indicates the square pyramidal geometry of the complexes.[47]

2.5 X-ray diffraction spectroscopy (XRD)

The XRD spectra of chitosan (CS) and deacetylated (~97%) chitosan (DCS) were analysed, and the peaks for CS appeared at $2\theta = 9^\circ$, 11.80° and 20.24°. After deacetylation, DCS showed two characteristic peaks at $2\theta = 10.65^\circ$ and 19.94° due to the formation of free amine (–NH_2) in CS.[48]

The XRD patterns of the Schiff bases were observed at $2\theta = 22.30^\circ$ and 22.39° for SB_1 and SB_2, respectively, indicating the formation of a Schiff base imine. The XRD patterns clearly reveal for complexes [(SB_1)–$Cu(OAc)_2$] and [(SB_2)–$Cu(OAc)_2$], that the crystalline index of the Schiff base ligand SB_1 at $2\theta = 22.30^\circ$ shifted to $2\theta = 16.20^\circ$, and for Schiff base ligand SB_2, $2\theta = 22.39^\circ$ was shifted to $2\theta = 16.15^\circ$ due to the π–π conjugation between the ligand and metal. The modification of DCS such as carboxymethylation, Schiff base formation and complexation decreased the crystallinity of the polymer due to the breakdown of the inter and intramolecular hydrogen bonding. The XRD pattern of the Cu(II) complexes showed peak broadening, which reveals that the hydrazide-based carboxymethyl chitosan strongly conjugated with the metal ion, as shown in Fig. 3. The crystallinity value of the starting material DCS compared to that of the Cu(II) complexes decreased due to the strong insertion of metal ion in the complexes.[49–51]

The crystalline indices (%) of DCS, ligands SB_1 and SB_2 and their Cu(II) metal complexes were calculated using the formula:

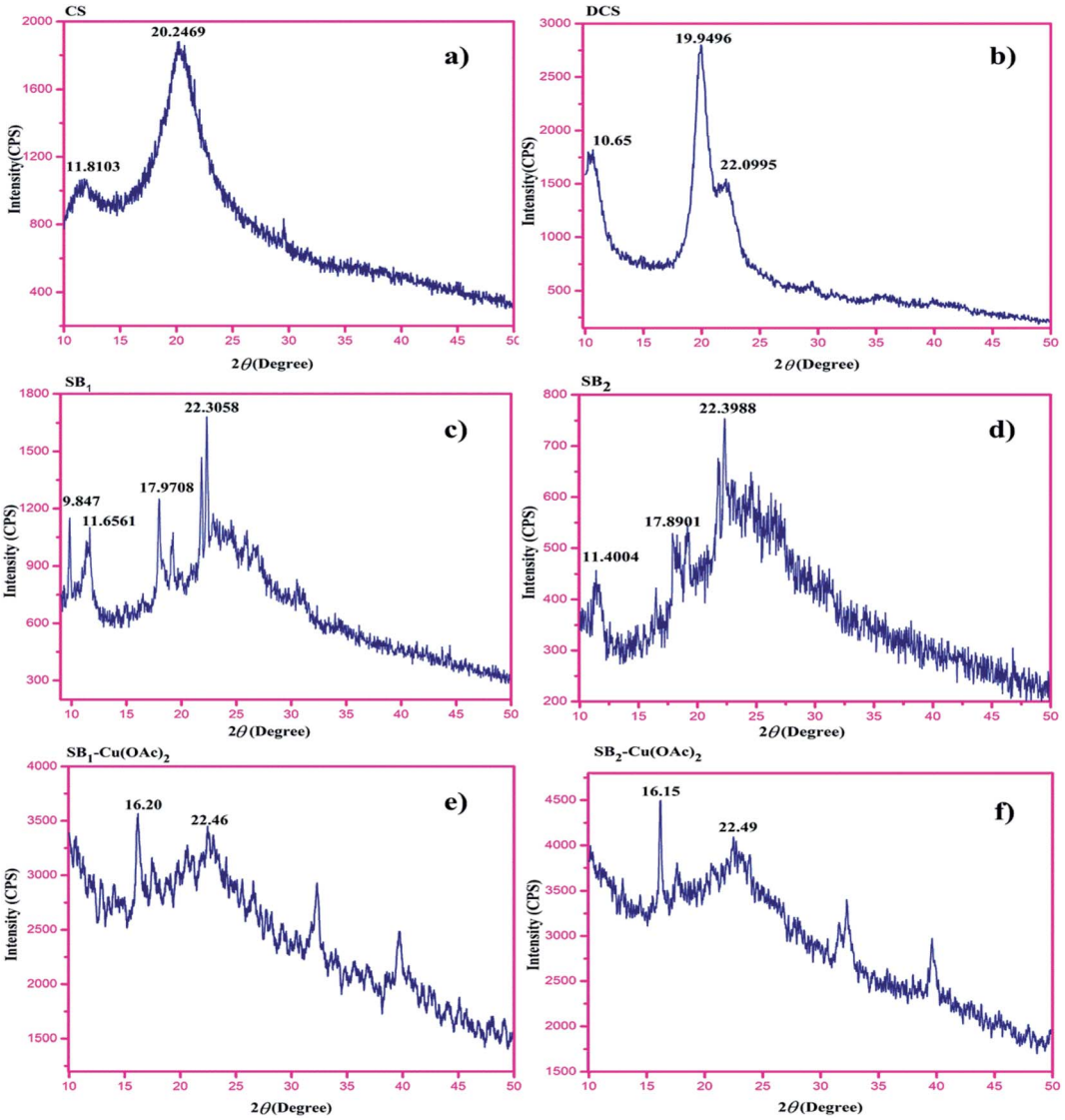

Fig. 3 X-ray diffraction patterns of (a) CS, (b) DCS, (c) SB_1, (d) SB_2, (e) SB_1–$Cu(OAc)_2$, and (f) SB_2–$Cu(OAc)_2$.

$$\%\ \text{of crystalline index} = \left[\frac{(I_{110} - I_{am})}{I_{110}}\right] \times 100 \qquad (3)$$

where I_{110} is the maximum intensity ~22.3° and I_{am} is the amorphous diffraction intensity for SB_1 = 16.20° and for SB_2 = 16.15°. The calculated crystalline index of the synthesized SB_1 and SB_2 of the Cu(II) complex is ~27% and ~28%, respectively.

2.6 TGA-DTA studies

The TGA-DTA curves of the deacetylated chitosan (DCS), *O*-carboxymethyl chitosan Schiff base ligands SB_1 and SB_2 and their Cu(II) complexes are shown in Fig. 4. The thermal decomposition of DCS (Fig. 4a) exhibited weight loss at 0 to 200 °C, 200 °C to 400 °C and >400 °C of 13.43%, 48.90% and 14.15%, respectively, which is in good agreement with the previous reports.[52]

The TGA-DTA curves of the Schiff base ligands (SB_1 and SB_2) are shown in Fig. 4b and c, respectively. The thermal curves of the Schiff bases exhibited their lower thermal stability than that of DCS. This change may be due to the coordination between the precursor and DCS. In addition, the chemical modification/Schiff base formation was also confirmed by the residue content of the Schiff base ligands, where they exhibited a higher residue content than that for the fully deacetylated chitosan (DCS).[53]

The TGA-DTA curve of the complex [SB_1–$Cu(OAc)_2$] (Fig. 4d) was examined, and a mass loss of about 11.61% was observed between 0–150 °C, which may be attributed to the loss of water and carboxymethyl groups. The mass loss of about 44.46% occurred between 150–400 °C due to the deformation of the Schiff base ligand and acetate units. The mass loss of about 8.21% occurred at the temperature of 400–800 °C due to the metal oxide residue. Thus, the TGA-DTA results reveal that the thermal stability and crystallinity of the synthesized Schiff base ligands and the complexes were lower than that of the initial chitosan.

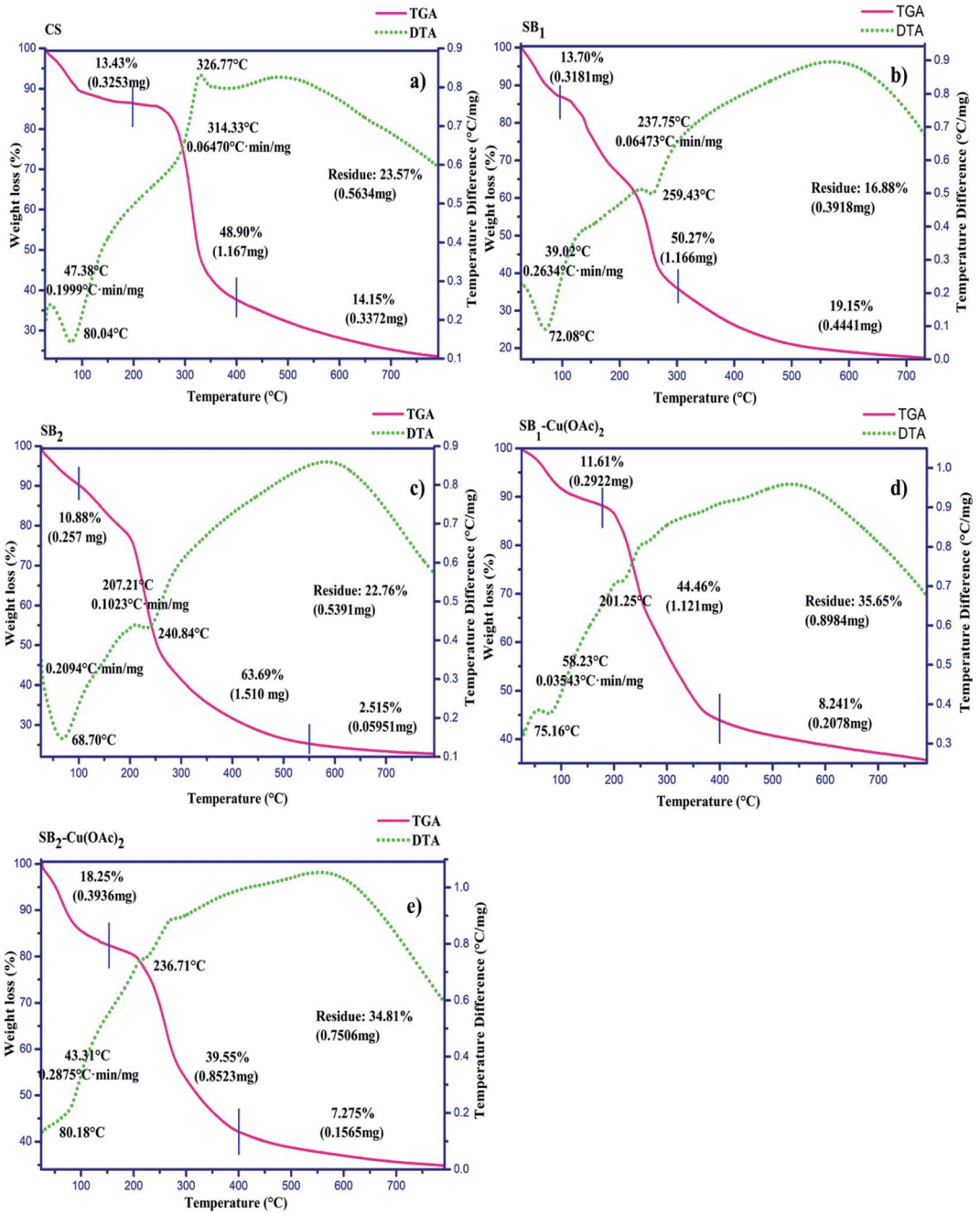

Fig. 4 TGA-DTA curves of (a) DCS, (b) SB_1, (c) SB_2, (d) SB_1–$Cu(OAc)_2$, and (e) SB_2–$Cu(OAc)_2$.

The TGA-DTA curve of complex [SB_2–$Cu(OAc)_2$] is shown in Fig. 4e. The mass loss about 18.25% occurred between 0–100 °C can be attributed to the loss of hydration and thermal degradation of the carboxymethyl group in the complex. The mass loss of about 39.55% occurred at a temperature between 100–400 °C, which can be attributed to the thermal breakdown of the Schiff base ligand and coordinated acetate units. The minimum mass loss (7.2%) occurred between 400–800 °C due to the metal oxide (CuO) residue. Substitution in the chitosan resulted in a loss of crystallinity in its backbone structure, thereby resulting in poor thermal stability and crystallinity. Subsequently, the thermal stability was enhanced due to the formation of complexes between the NNO tridentate ligand (SB_1 or SB_2) and Cu(II) ion, which may be due to the metal oxide (CuO) residue in the complexes. The enhanced thermal stability of metal complexes was extended at wide range of temperature range.[54] The thermogravimetric study indicates that the fully deacetylated chitosan (DCS) was more thermally stable than the *O*-CMCS Schiff base ligand and their Cu(II) complexes.[55] The thermal stability of the complexes followed the order of:

Thermal stability

Chitosan > [(SB_1)–$Cu(OAc)_2$] – [(SB_2)–$Cu(OAc)_2$] > (SB_1) – (SB_2)

2.7 SEM-EDAX

The SEM images of chitosan and 4-hydroxy benzohydrazide-grafted biopolymer Schiff base ligands (SB_1 and SB_2) and their Cu(II) complexes are shown in Fig. 5. The SEM image of chitosan shows that its morphology was regular and homogenous and it possessed a smooth surface. The formation of Schiff base and carboxymethylation in chitosan led to moisture absorbing characteristics, which are beneficial for its use in cosmetics, pharmaceutical, biomedical and other biological applications. The homogeneous surface of chitosan became rough and porous due to the chemical modification of primary alcohol and amine groups in its saccharide ring.[56]

The complexation between the hydrazide-grafted *O*-carboxymethyl chitosan Schiff base ligand and metal ion caused the surface of the material to become more rough, regular and amorphous. The particle size, roughness and porous structure of the ligands dramatically changed after the formation of the complexes. The SEM images of Cu(II) complexes exhibited a uniform, regular, amorphous and layered structure, which reveals that the complexes have potential antimicrobial, anti-inflammatory, antidiabetic and total antioxidant activities.[57]

The Cu(II) complexes were also examined *via* energy dispersive X-ray spectroscopy (EDAX) and the results are shown in Fig. 6. The EDAX spectra of the hydrazide incorporated *O*-carboxymethyl chitosan Schiff base ligands (SB_1 and SB_2) and their Cu(II) acetate complexes confirm the presence of C, N and O atoms with their weight percentages. The EDAX spectra made it possible to verify the presence of the metallic species in the samples, confirming the metal ion insertion in the complexes.[58–60]

2.8 Electron spin resonance (ESR) spectroscopic studies

ESR spectroscopy was used to characterise the species that contained unpaired electrons (free radicals, transition metal complexes, odd-electron molecules, rare earth ions, *etc.*) in the chemical structure of the complexes and facilitated investigation of the electron spin and oxidation state of the metal ion coordinating with the Schiff base ligand. The ESR spectra of the complexes revealed hyperfine and super hyperfine

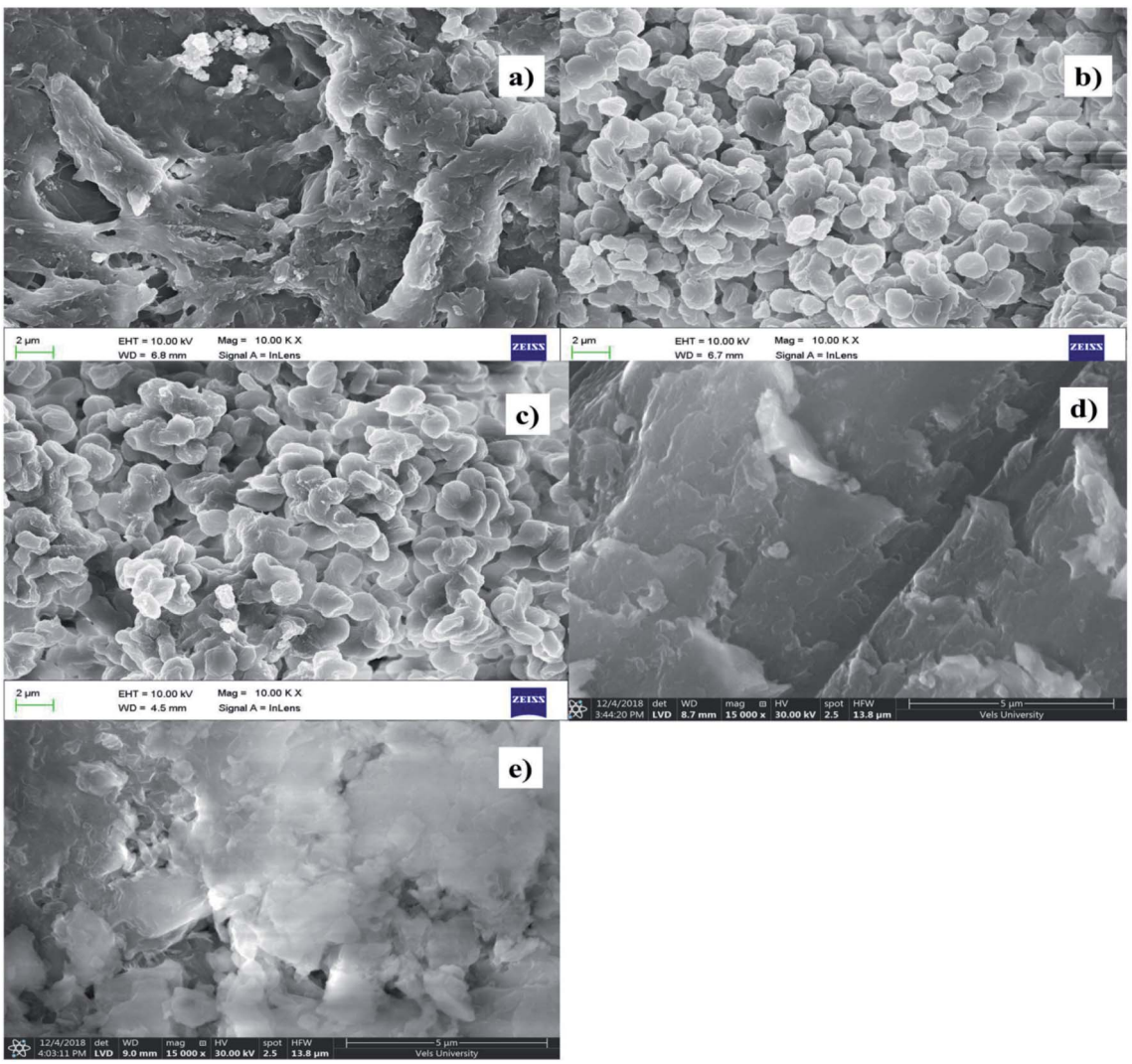

Fig. 5 SEM images of (a) DCS, (b) SB_1, (c) SB_2, (d) SB_1–$Cu(OAc)_2$, and (e) SB_2–$Cu(OAc)_2$.

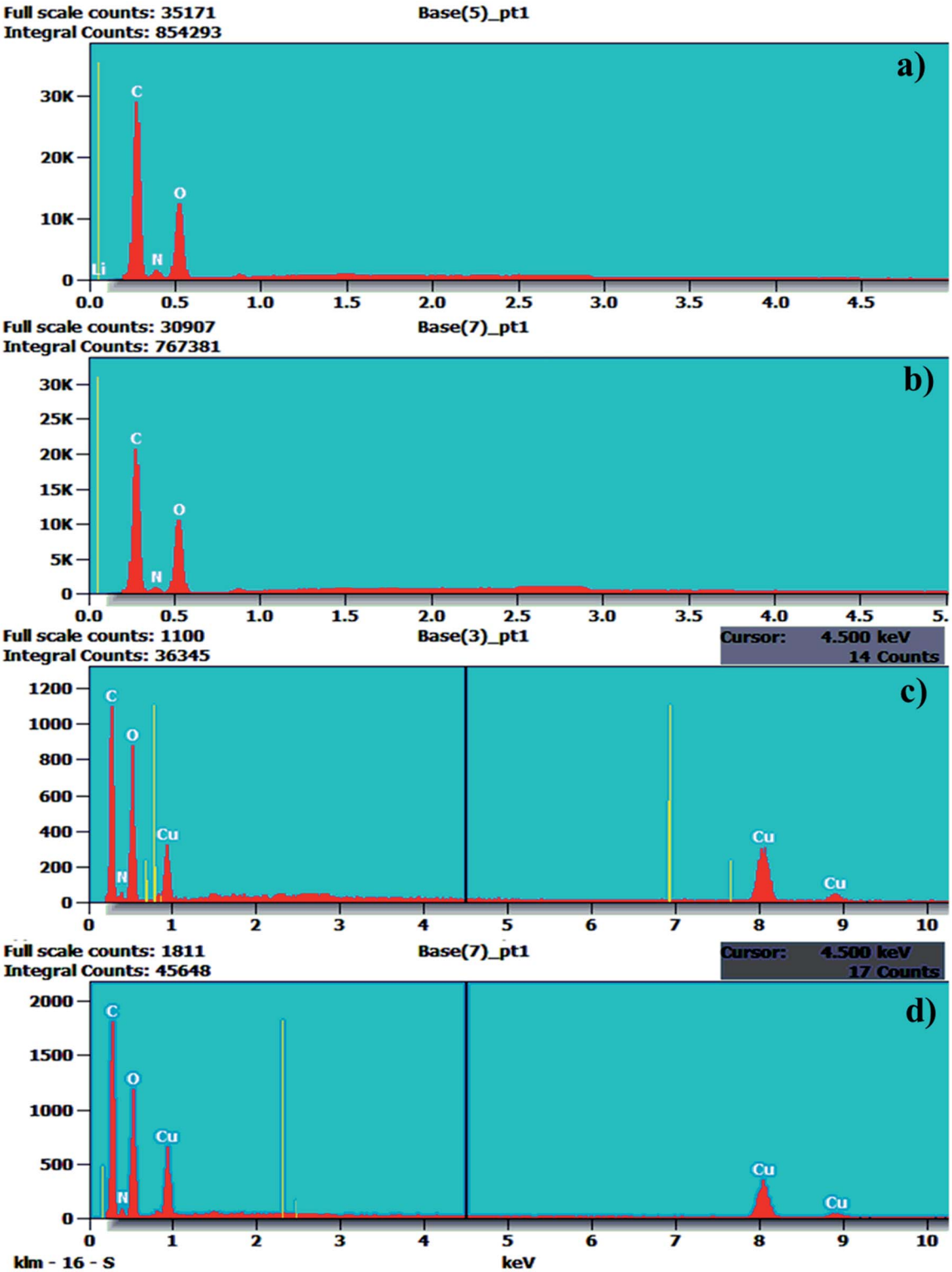

Fig. 6 EDAX spectra of (a) SB_1, (b) SB_2, (c) SB_1–$Cu(OAc)_2$, and (d) SB_2–$Cu(OAc)_2$.

structures, confirming the environment of the metal ion in the complexes, which are related to the geometry and degree of covalence in the complexes, respectively. The ESR spectra of the complexes were recorded to investigate the metal–ligand bonding, which helped determine the magnetic interaction of the metal complexes.[61]

The spectra of the powder complexes were recorded at room temperature (300 K). Fig. 7 shows that the ESR spectra of the complexes exhibit an axial signal with two g values ($g_{\|} = 2.169$ and $g_{\perp} = 2.081$) for [SB_1–$Cu(OAc)_2$] and ($g_{\|} = 2.132$ and $g_{\perp} = 2.028$) [SB_2–$Cu(OAc)_2$]. The g value of the complexes was >2.0023, where this low g value of the Cu(II) ions exhibits

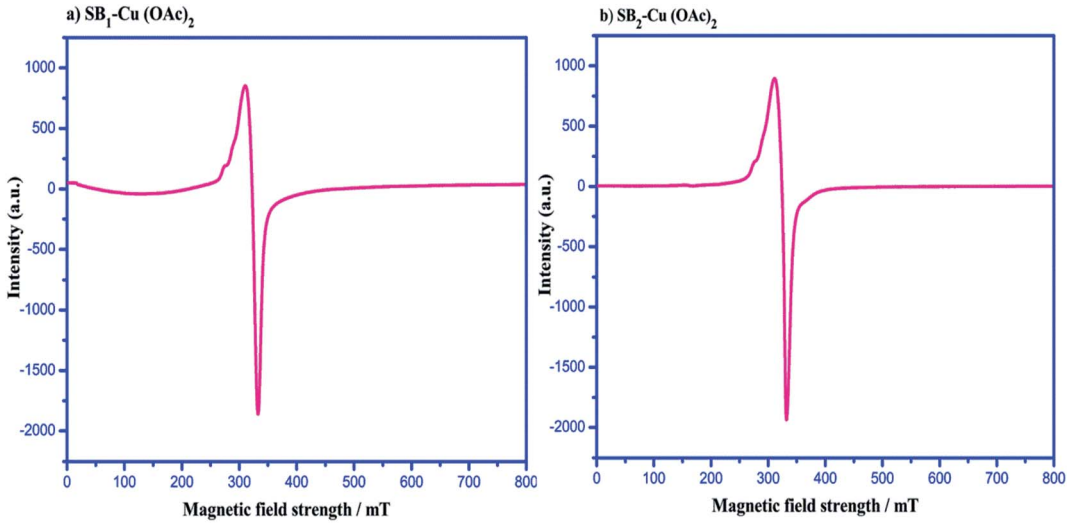

Fig. 7 Electron spin resonance spectra of (a) SB_1–$Cu(OAc)_2$ and (b) SB_2–$Cu(OAc)_2$.

John–Teller distortion due to the Cu(II) ions existing in an axial symmetry with all the principal axes aligned parallel to the distorted octahedral geometry. The G factor values $[(g_{\parallel} - 2)/(g_{\perp} - 2)] = 2.09$ for $[SB_1$–$Cu(OAc)_2]$ and $[(g_{\parallel} - 2)/(g_{\perp} - 2)] = 4.71$ for $[SB_2$–$Cu(OAc)_2]$ indicate the presence of slight misalignment in the tetragonal axes and negligible exchange interactions between the Cu(II) centers. The g values of the complexes followed the order of $g_{\parallel} > g_{\perp} > 2.0023$. This reveals that the unpaired electrons of the complexes were present in the $d_{x^2-y^2}$ orbital. The Cu(II) complexes showed $g_{\parallel} < 2.3$, which demonstrated the covalent character of the metal–ligand interactions.[62]

2.9 Magnetic measurement

The magnetic measurements for the Cu(II) complexes were performed at room temperature for complexes $[(SB_1)$–$Cu(OAc)_2]$ and $[(SB_2)$–$Cu(OAc)_2]$, which had a d^9 electronic configuration with a paramagnetic nature. The magnetic moment of these two Cu(II) complexes was found to be 1.87 BM and 1.83 BM, respectively. The resulting BM values of Cu(II) complexes confirm the presence of an unpaired electron, and thus their paramagnetic nature. Furthermore, the magnetic moment values of the complexes prove that the coordination number of the complexes is five and they have square pyramidal geometry.[63]

2.10 Molar conductivity measurements

The molar conductance values of 0.001 M solution of complexes [3a-OCMCS $Cu(OAc)_2$] and [3b-OCMCS $Cu(OAc)_2$] were in the range of 14 to 24 ohm^{-1} cm^2 mol^{-1}. These values indicate that the complexes are non-electrolytic in nature.[64] The observed molar conductance of the complexes were as follows: $[SB_1$–$Cu(OAc)_2$: 19 Ω^{-1} cm^2 $mol^{-1}]$ and $[SB_2$–$Cu(OAc)_2$: 16 Ω^{-1} cm^2 $mol^{-1}]$.

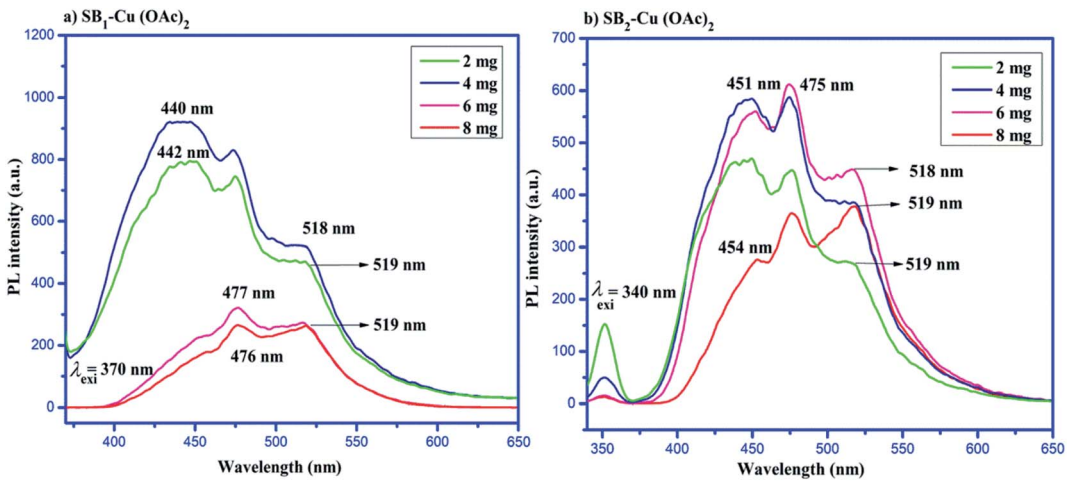

Fig. 8 Photoluminescence spectra of (a) SB_1–$Cu(OAc)_2$ and (b) SB_2–$Cu(OAc)_2$.

Table 3 Excitation wavelength-dependent emissions of the 4-hydroxy benzohydrazide-based biopolymer/*O*-carboxymethyl chitosan Schiff Cu(II) complexes

Name of the compounds	Catalytic dosage (mg)	Excitation wavelength λ_{exi} (nm)	Emission wavelength λ_{emi} (nm)	Stokes shift	PL intensity	
[(SB_1)–$Cu(OAc)_2$]	2	386	442	56	793	Increase
	4	385	440	55	921	
	6	420	477	57	322	Decrease
	8	423	476	54	265	
[(SB_2)–$Cu(OAc)_2$]	2	398	452	51	469	Increase
	4	399	451	52	588	
	6	400	450	50	612	
	8	405	454	49	377	Decrease

2.11 Photoluminescence (PL) studies

The photoluminescence (PL) spectra of the Cu(II) complexes of SB_1 and SB_2 are shown in Fig. 8. The emission spectra of different concentrations of the complexes (SB_1–$Cu(OAc)_2$ and SB_2–$Cu(OAc)_2$) were recorded at 25 °C in DMSO by exciting the complexes at the wavelengths of 370 nm and 340 nm, respectively.[65] The maximum excitation and emission wavelengths (nm) of the catalysts are presented in Table 3. Specifically, 2 mg of SB_1–$Cu(OAc)_2$ complex showed emission at 442 nm upon excitation at 386 nm, showing a Stokes shift of 56 nm, 4 mg of SB_1–$Cu(OAc)_2$ complex showed emission at 440 nm upon excitation at 385 nm with a Stokes shift of 55 nm, 6 mg of SB_1–$Cu(OAc)_2$ complex showed emission at 477 nm upon excitation at 420 nm with a Stokes shift of 57 nm, and 8 mg of SB_1–$Cu(OAc)_2$ complex showed emission at 476 nm upon excitation at 423 nm with a Stokes shift of 54 nm. These bands can be attributed to the $\pi \rightarrow \pi^*$ electronic transition.

Similarly, the emission band appeared at 449 nm for SB_2–$Cu(OAc)_2$ (2 mg) when the catalyst was excited at 398 nm with a Stokes shift of 51 nm, the emission band appeared at 399 nm for SB_2–$Cu(OAc)_2$ (4 mg) when the catalyst was excited at 451 nm with a Stokes shift of 52 nm, the emission band appeared at 450 nm for SB_2–$Cu(OAc)_2$ (6 mg) when catalyst was excited at 400 nm with a Stokes shift of 50 nm and the emission band appeared at 454 nm for SB_2–$Cu(OAc)_2$ (8 mg) when the catalyst was excited at 405 nm with a Stokes shift of 49 nm.[66] The emission of the complexes with high concentration showed a blue shift to a lower wavelength. These observed lower wavelengths resulted in lower Stokes shift values. Moreover, the PL intensity of the emission bands decreased in the metal complexes due to the quenching effect. This reveals that charge transfer occurred in the excited state, leading to a quenching effect in the emission band.[67]

2.12 Photocatalytic dye degradation of methylene blue (MB)

The degradation of the organic dye methylene blue was evaluated with and without the catalyst under ultraviolet light irradiation. The degradation of the dye using the catalyst was carried out at different time intervals in a dark room. The catalysts showed no change in the dye degradation rate, and the observed adsorption curves are shown in Fig. 9. However, when the catalyst was exposed to UV light irradiation at different catalyst doses, at different medium pH and different durations, degradation was observed. About 5 to 20 mg of catalyst was used to optimize the degradation experiment. The degradation efficiency of about 86.63% for MB was achieved at with a 20 mg dose of SB_1–$Cu(OAc)_2$ and about 92.38% with 20 mg of SB_2–$Cu(OAc)_2$, as shown in Fig. 10a. The photocatalytic degradation

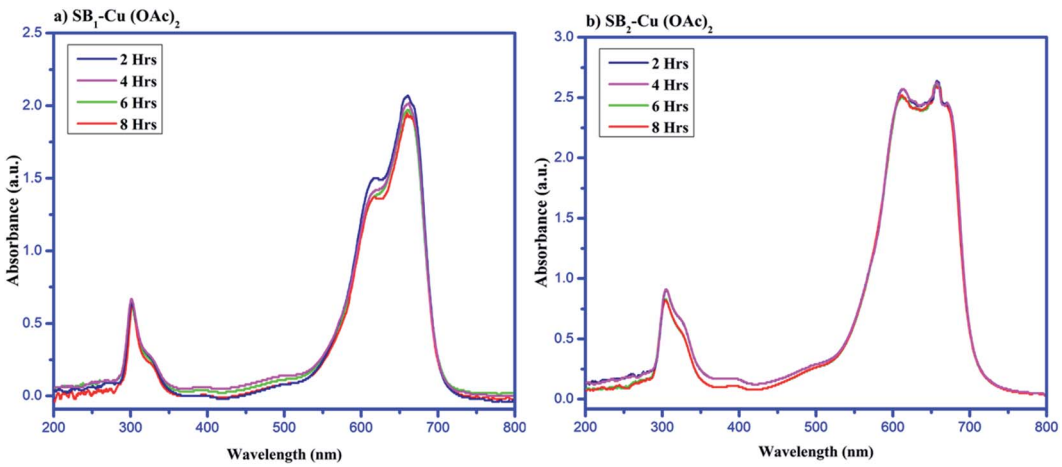

Fig. 9 Methylene blue degradation by (a) SB_1–$Cu(OAc)_2$ and (b) SB_2–$Cu(OAc)_2$ catalysts in the dark.

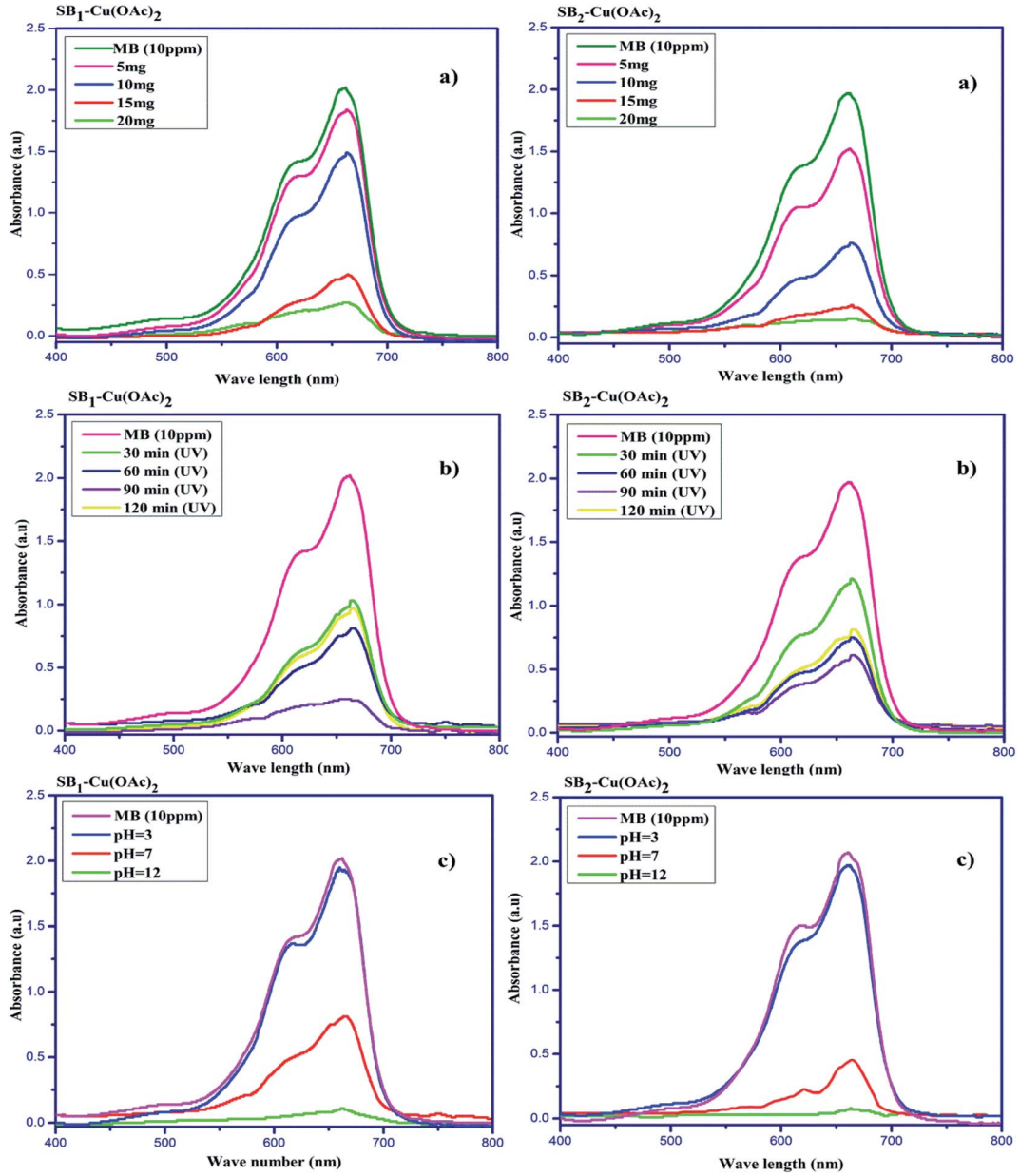

Fig. 10 Photocatalytic degradation of methylene blue using the biopolymer Cu(II) complexes with respect to (a) catalyst dosage, (b) irradiation time and (c) pH variation.

depends on the amount catalyst, *i.e.* an increase in the number of active sites on the catalytic surface increases the degradation.[68,69] The order of the photocatalytic efficiency of the catalysts at different dosages is shown in Fig. 11a.

Similarly, the photocatalytic degradation of MB was investigated under UV irradiation for 120 min for catalysts I and II. Fig. 10b shows the absorption spectra of aqueous MB under the influence of the SB_1–$Cu(OAc)_2$ and SB_2–$Cu(OAc)_2$ catalysts for different periods. The SB_1–$Cu(OAc)_2$ catalyst showed an absorbance of about 59.90% in 60 min and SB_2–$Cu(OAc)_2$ about 69.03% in 90 min. After 90 minutes of UV irradiation, no considerable change in dye degradation occurred.[70] The order of the photocatalytic efficiency of the catalysts for difference irradiation times is shown in Fig. 11b.

Fig. 10c shows the dye degradation efficiency of SB_1–$Cu(OAc)_2$ and SB_2–$Cu(OAc)_2$ at acidic, neutral and basic pH values since pH also plays an important role in the photocatalytic degradation of MB. At pH = 12, the SB_1–$Cu(OAc)_2$ catalyst showed an absorbance of about 94.55% in 60 min and SB_2–$Cu(OAc)_2$ about 96.11% in 90 min.

The dye degradation studies confirmed that the aryl-substituted (SB_2–$Cu(OAc)_2$) catalyst exhibited better dye degradation than that of the aliphatic-substituted catalyst (SB_1–$Cu(OAc)_2$), as shown in Fig. 11. The 4-hydroxy benzohydrazide metal complexes produced hydroxyl radicals, which act as

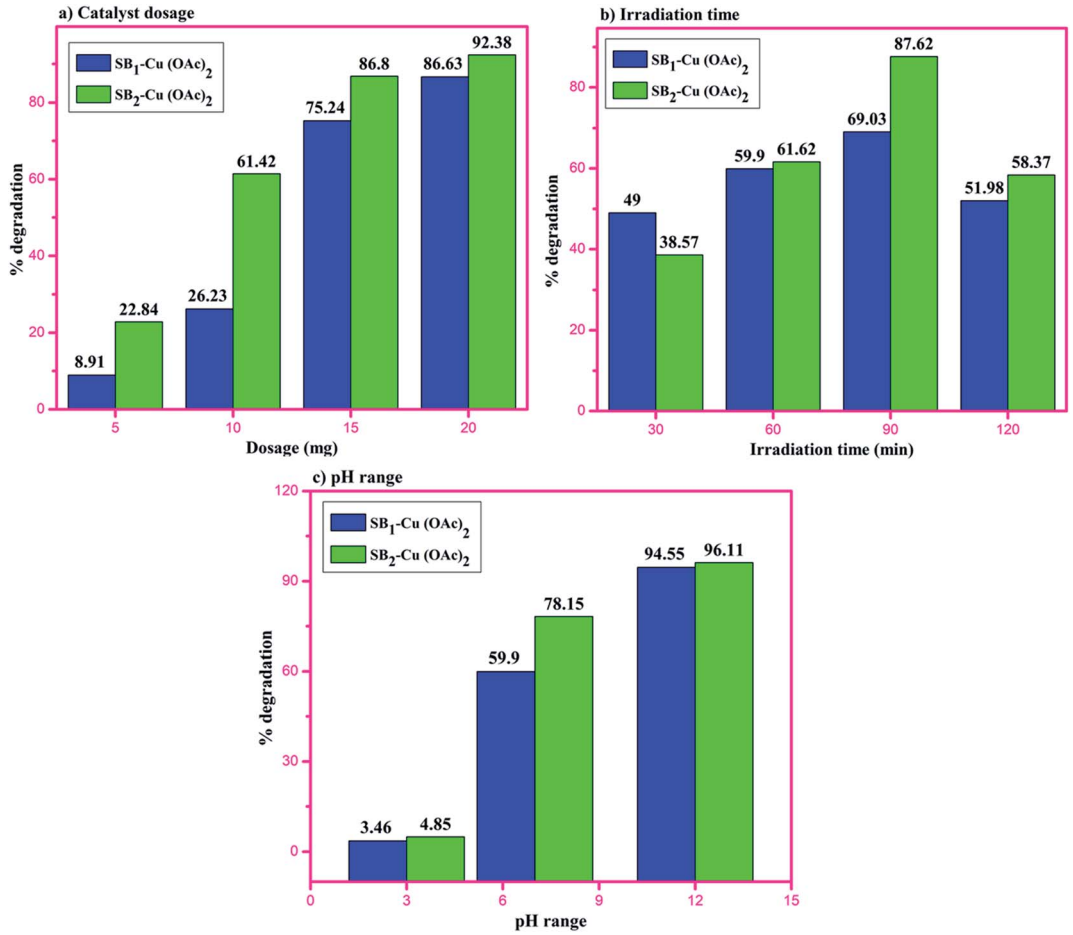

Fig. 11 Order of the photocatalytic efficiency of the catalysts at different (a) dosages, (b) irradiation times and (c) pH.

oxidizers in the photo-induced degradation of organic pollutants.[71] Therefore, the effect of alkaline pH (12), at 60 min of irradiation for 15 mg catalyst I and at 90 min of irradiation for 10 mg catalyst-II resulted in the best photocatalytic degradation of methylene blue. The order of the photo catalytic efficiency of the catalysts at different pH is shown in Fig. 11c. Generally, metal-based catalysts play an important role in the degradation of dyes due to their photo-sensitization and electron conduction properties. These properties of the present eco-friendly biopolymer catalyst resulted in better dye degradation than that of the reported compounds, as shown in Table 4.[72–75]

The tentative mechanism for the photocatalytic degradation of methylene blue is shown in Fig. 12.[70]

$$C_1 = [SB_1\text{–}Cu(OAc)_2],\ C_2 = [SB_2\text{–}Cu(OAc)_2]$$

$$M^{2+} \rightarrow M^{+} + H^{+} + \cdot OH \text{ (hydroxyl radical)}$$

$$[C_1] \text{ or } [C_2] + 2H_2O \xrightarrow{h\nu(\text{UV-light})} [SB_1 - Cu(H_2O)_2] \text{ or } [SB_2 - Cu(H_2O)_2] + 2CH_3COO^{\bullet}$$

$$CH_3COO^{\bullet} + NaOH \rightarrow CH_3COONa + \cdot OH$$

$$MB + \cdot OH \rightarrow \text{degradation products } (CO_2 \text{ and } H_2O).$$

Table 4 Comparison of the present work with reported photocatalysts

Substrate	Catalyst	Dye degradation (%)	Degradation time (min)	Recyclability	Reference
RB-5	Hybrid Cu(II)OCMC	93	130	3	72
MB	Cu_2O nanoparticles	63	80	—	73
RHB	CuL	89	60	—	74
MB	Hybrid Cu(II) $PMo_{12}O_{40}^{3-}$	96	240	3	75
MB	SB_2–$Cu(OAc)_2$	87	90	4	Present work
MB	SB_2–$Cu(OAc)_2$ (pH = 12)	96	90	4	

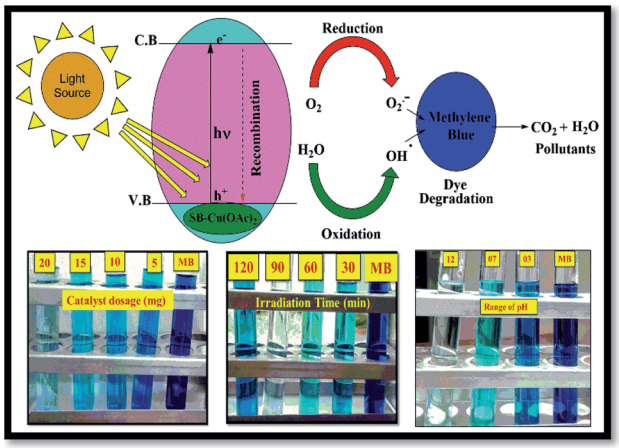

Fig. 12 Photocatalytic degradation of methylene blue under UV-visible irradiation.

2.13 Reusability

Low cost, easily availability and non-conventional biopolymer photocatalysts play an important role in the dye degradation process. A significant decrease in dye degradation was not observed after four continuous cycles. The catalysts were recycled to an extent of 88% for the dye degradation process. The decrease in the percentage degradation efficiency is related to the loss of photocatalyst during the sample handling and centrifugation process. After four cycles of dye degradation, the SEM images (Fig. 13a and b) showed a dramatic change and the weight percentage of the composition of elements in the EDAX spectra also changed, as shown in Fig. 13c and d, respectively. Besides, the X-ray diffractograms of the catalysts (Fig. 13e and f) showed aggregated peaks, which revealed the presence of dye particles in the catalysts. The percentage photocatalytic dye degradation by the biopolymer metal complexes is shown in Fig. 13g.

2.14 Biological activity

The biopolymer Schiff base ligands (SB_1 and SB_2) and their metal complexes [(SB_1)–$Cu(OAc)_2$] and [(SB_2)–$Cu(OAc)_2$, respectively] were studied for their anti-inflammatory activity using the egg albumin denaturation technique and antidiabetic activity using the McCue and Shetty method, as shown below.

2.14.1 Anti-inflammatory activity (egg albumin denaturation technique). The anti-inflammatory activity results for SB_1, SB_2, SB_1–$Cu(OAc)_2$ and SB_2–$Cu(OAc)_2$ are displayed in Fig. 14. The SB_1–$Cu(OAc)_2$ drug showed a maximum inhibition of 91.45 ± 3.0% at the maximum concentration of 500 μg mL^{-1}. The anti-inflammatory activity of SB_1–$Cu(OAc)_2$ was better than that of the reported Schiff base complexes. The anti-inflammatory (BSA) denaturation activity is reported in terms of percentage inhibition for SB_1, SB_2, SB_1–$Cu(OAc)_2$ and SB_2–$Cu(OAc)_2$, with maximum values of 82.55% ± 2.6%, 81.79% ± 2.5%, 91.45% ± 3.0% and 86.35% ± 2.8%, respectively. The SB_1–$Cu(OAc)_2$ compound showed a better anti-inflammation effect compared to diclofenac sodium.[76]

2.14.2 Antidiabetic assay (McCue and Shetty method). The antidiabetic activities were studied for all the synthesized biopolymer Schiff bases and the reference drug acarbose. The Schiff base metal complexes showed better antidiabetic results than their corresponding Schiff base ligands.

The antidiabetic effects were measured in terms of percentage inhibition for SB_1, SB_2, SB_1–$Cu(OAc)_2$ and SB_2–$Cu(OAc)_2$, with maximum values of 82.46% ± 2.6%, 88.72% ± 2.9%, 84.93% ± 2.7% and 93.13% ± 3.2%, respectively.[77] However, the presence of the aromatic substituent and phenolic function in complex SB_2–$Cu(OAc)_2$ resulted in better activity compared to that of the standard drug acarbose, as shown in Fig. 15.

3. Experimental

3.1 Materials and methods

Chitosan (90% deacetylated), acetyl acetone, dibenzoyl methane, monochloroacetic acid, copper(II) acetate monohydrate, 4-hydroxy benzohydrazide, methanol, acetic acid, methylene blue and sodium hydroxide were purchased from Sigma Aldrich and SRL India and used as supplied without further purification.

3.1.1 Determination of solubility. Solubility studies were performed to determine the solubility/insolubility of the complexes in various solvents. The solubility was determined by a naked eye detection method. About 10 mg of synthesized compound was dissolved in 1 mL of various solvents including DMSO, DMF, MeOH, ethanol, water and $CHCl_3$ and allowed to cool at room temperature.

3.1.2 Elemental analysis. Deacetylated chitosan (DCS), the synthesized biopolymer Schiff base ligands (SB_1 and SB_2) and their Cu(II) complexes contained the elements C, H, and N, and their weight percentages were determined using a CHNS/O Analyser (2400 Series II, PerkinElmer).

3.1.3 FT-IR analysis. Fourier-transform infrared (FT-IR) spectra were recorded for chitosan (90%), DCS (97%), the Schiff base ligands (SB_1 and SB_2) and their Cu(II) complexes using a PerkinElmer Spectrum Version 10.4.00 with KBr pellets in the wavenumber range of 4000–400 cm^{-1}.

3.1.4 ^{1}H NMR and ^{13}C NMR. ^{1}H and ^{13}C Fourier-transform nuclear magnetic resonance (FT-NMR) spectra were recorded and analysed for SB_1 and SB_2 at 20 °C using a Bruker Ultrashield NMR spectrometer operating at 400 MHz and deuterated water (D_2O) as the solvent at a concentration of 15 mg mL^{-1}.

3.1.5 Ultraviolet-visible analysis. The electronic spectra of the Schiff bases (SB_1 and SB_2) and their Cu(II) complexes were analysed using a Flame UV-vis fibre optic Spectrophotometer. The as-synthesized Schiff base ligands and their Cu(II) complexes were dissolved in water and DMSO at a concentration of 10 mg mL^{-1}.

3.1.6 X-ray powder diffraction studies (XRD). X-ray diffractograms were recorded for the synthesized compounds using a 2.2 kW-Cu-anode ceramic tube with a LYNXEYE detector (silicon strip detection) and scintillation Detector (for low angle

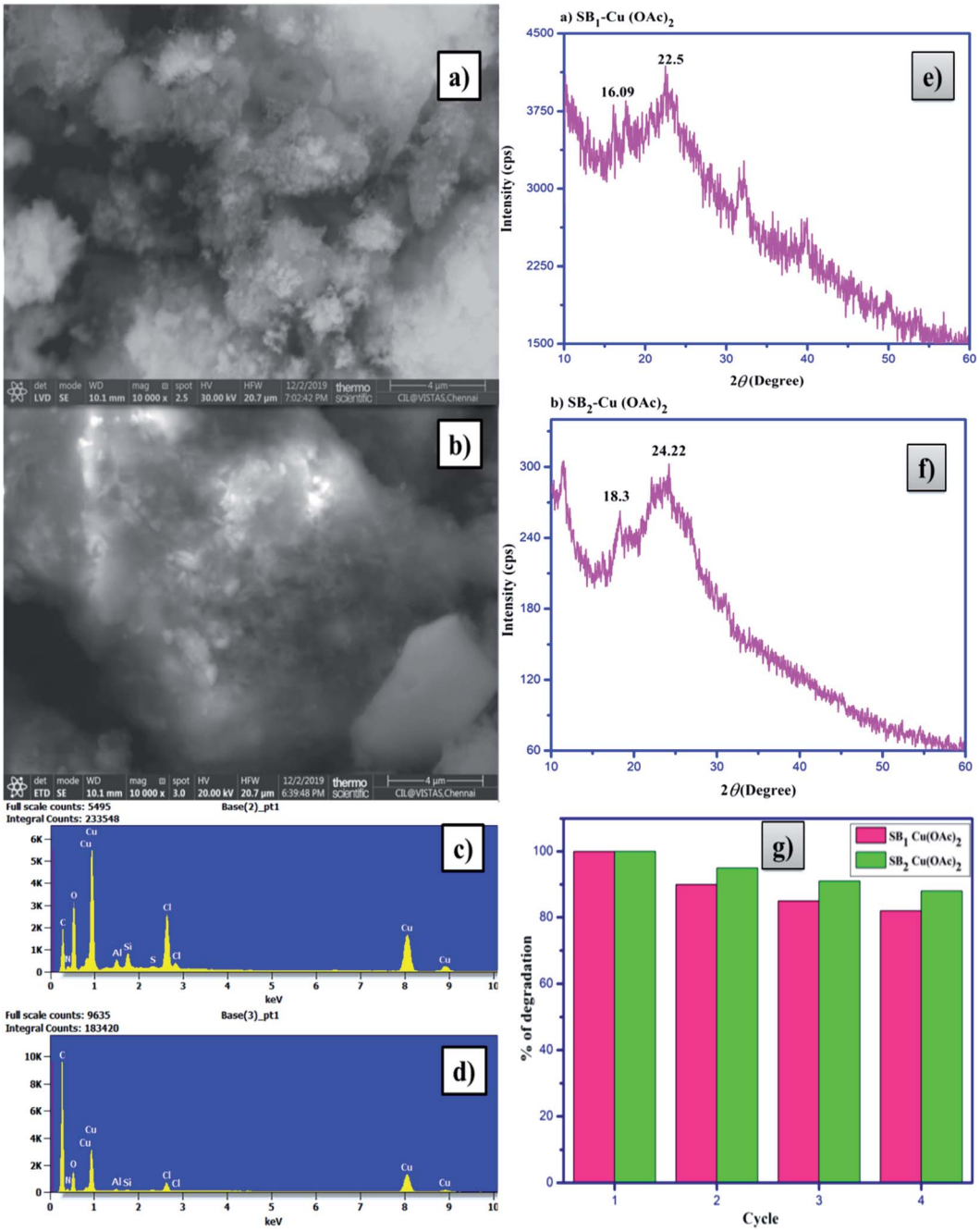

Fig. 13 SEM images of (a) SB_1–$Cu(OAc)_2$ and (b) SB_2–$Cu(OAc)_2$, EDAX spectra of (c) SB_1–$Cu(OAc)_2$ and (d) SB_2–$Cu(OAc)_2$, XRD patterns of (e) SB_1–$Cu(OAc)_2$ and (f) SB_2–$Cu(OAc)_2$, and (e) reusability of the biopolymer photocatalysts after four cycles of dye degradation.

XRD analysis). The patters were recorded in the 2θ range of 10° to 90° with a potential difference of 40 kV and current of 30 mA using Cu kα radiation at $\lambda = 0.15406$ nm at a scan rate of 0.02° min^{-1} using a Bruker D8 Advance XRD, Germany.

3.1.7 Thermogravimetric analysis and differential thermal analysis (TGA-DTA). Thermogravimetric analysis (TGA) and differential thermal analysis (DTA) were performed for the Schiff bases ligands (SB_1 and SB_2) and their Cu(II) complexes using an SDT Q-600, TGA-DTA modulus (from TA-Instruments, USA), with a sample mass of 2.0 mg in an alumina sample holder at a heating rate of 20 °C min^{-1}, under a flow of nitrogen gas (100 mL min^{-1}).

3.1.8 SEM (scanning electron microscopy) and EDAX (energy-dispersive X-ray spectroscopy). The SEM images of DCS, Schiff base ligands (SB_1 and SB_2) and their Cu(II) complexes were obtained using a ZEISS SIGMA FESEM with a gold and palladium QUORUM Sputter Coater sc7620. The EDAX spectra for the Schiff bases and their metal complexes were recorded using a Quattro S, ThermoFisher Scientific FEI Company of USA.

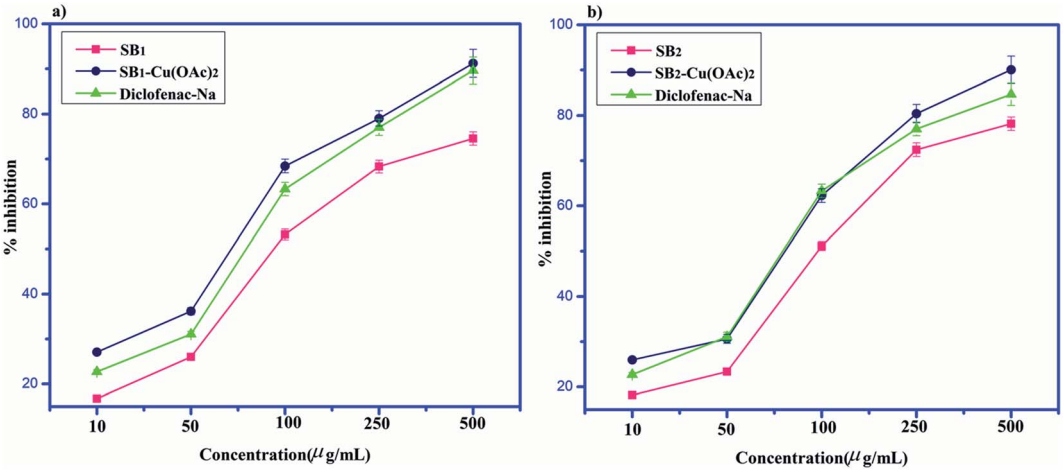

Fig. 14 Anti-inflammatory studies of (a) SB_1–$Cu(OAc)_2$ and (b) SB_2–$Cu(OAc)_2$.

3.1.9 Electron spin resonance (ESR) spectroscopic studies. ESR spectra were recorded for the complexes (SB_1–$Cu(OAc)_2$ and SB_2–$Cu(OAc)_2$) using an electron spin resonance spectrometer (JEOL Model JES FA200 instrument) operating at 8.75–9.65 GHz frequency (X-band) at 25 ± 2 °C.

3.1.10 Magnetic moments. Magnetic measurements were performed using a 7407-S Lakeshore cryogenic vibrating sample magnetometer (VSM), USA. The magnetic susceptibility (χ) = M/H values were studied at room temperature for the Cu(II) complexes of SB_1 and SB_2.

3.1.11 Molar conductivity studies. The molar conductivity of the *O*-carboxymethyl chitosan Schiff base Cu(II) complexes were studied at 25 ± 2 °C using a Table Top-Digital conductivity meter.

3.1.12 Photoluminescence (PL) studies. The photoluminescence of the synthesized *O*-carboxymethyl chitosan Schiff base Cu(II) metal complexes was recorded using a Horiba Jobin monochromator (330 nm and 550 nm) PMT detector.

3.1.13 Photocatalytic organic dye degradation studies. The photocatalytic dye degradation efficiency of the metal complexes (SB_1–$Cu(OAc)_2$ and SB_2– $Cu(OAc)_2$) was determined by the degradation of methylene blue. The degradation was measured both before and after 320 nm ultraviolet (UV) light irradiation on the mixture. Different doses of 5, 10, 15 and 20 mg of the prepared catalyst were mixed in 100 mL aqueous solution of methylene blue (10 mg/1000 mL). The prepared reaction suspension was allowed to react at ambient condition under constant stirring. After irradiation, the catalyst was separated by centrifugation and the absorbance of methylene blue was measured using a UV-visible spectrophotometer at 664 nm. The percentage photocatalytic activity was calculated using the following formula:

$$\text{Percentage of dye degradation} = \left[\frac{C_0 - C}{C_0}\right] \times 100 \qquad (4)$$

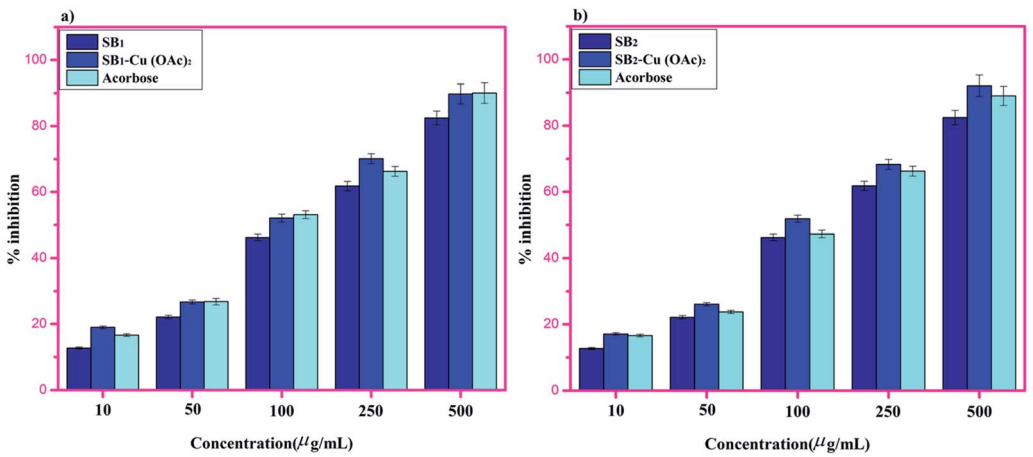

Fig. 15 Antidiabetic assay of (a) SB_1–$Cu(OAc)_2$ and (b) SB_2–$Cu(OAc)_2$.

where C_0 is the initial concentration of dye solution at 0 min (before the photocatalytic reaction), and C is the concentration of dye solution at a certain time (after the photocatalytic reaction).

3.1.14 Anti-inflammatory activity (egg albumin denaturation technique). Anti-inflammatory studies were performed for the biopolymer Schiff base ligands (SB_1 and SB_2) and their Cu(II) complexes using the egg albumin denaturation inhibition technique. All test samples were administered with diclofenac sodium (standard drug). The test samples were taken at different doses of 10, 50, 100, 250 and 500 μM dissolved in water and dimethyl formamide (DMF) with diluted phosphate buffer (0.2 M, pH = 7.4). About 4 mL of all the test solutions consisting of the minimum concentration (<2.5%) was mixed with 1 mL of 1% egg albumin solution in phosphate buffer. Finally, the mixture was kept in an incubator at 37 °C for 20 min followed by induction of egg albumin denaturation in the reaction mixture at 70 °C in a water bath for 20 min. Then, the mixture was allowed to cool to room temperature until turbidity was observed and then measurements were performed at 660 nm using a UV-spectrophotometer. The percentage egg albumin denature inhibition was calculated using the following formula:

$$\text{Percentage inhibition of egg albumin denaturation} = \left[\frac{A_t - A_c}{A_t}\right] \times 100 \quad (5)$$

where A_t and A_c are the absorbance of the test solution and control solution, respectively.

3.1.15 Antidiabetic (α-amylase inhibitory) studies. The antidiabetic activity of the as-synthesized 4-hydroxy benzohydrazide-based biopolymer Schiff bases and their Cu(II) complexes was studied using a modified McCue and Shetty method. All the prepared test samples were treated with the

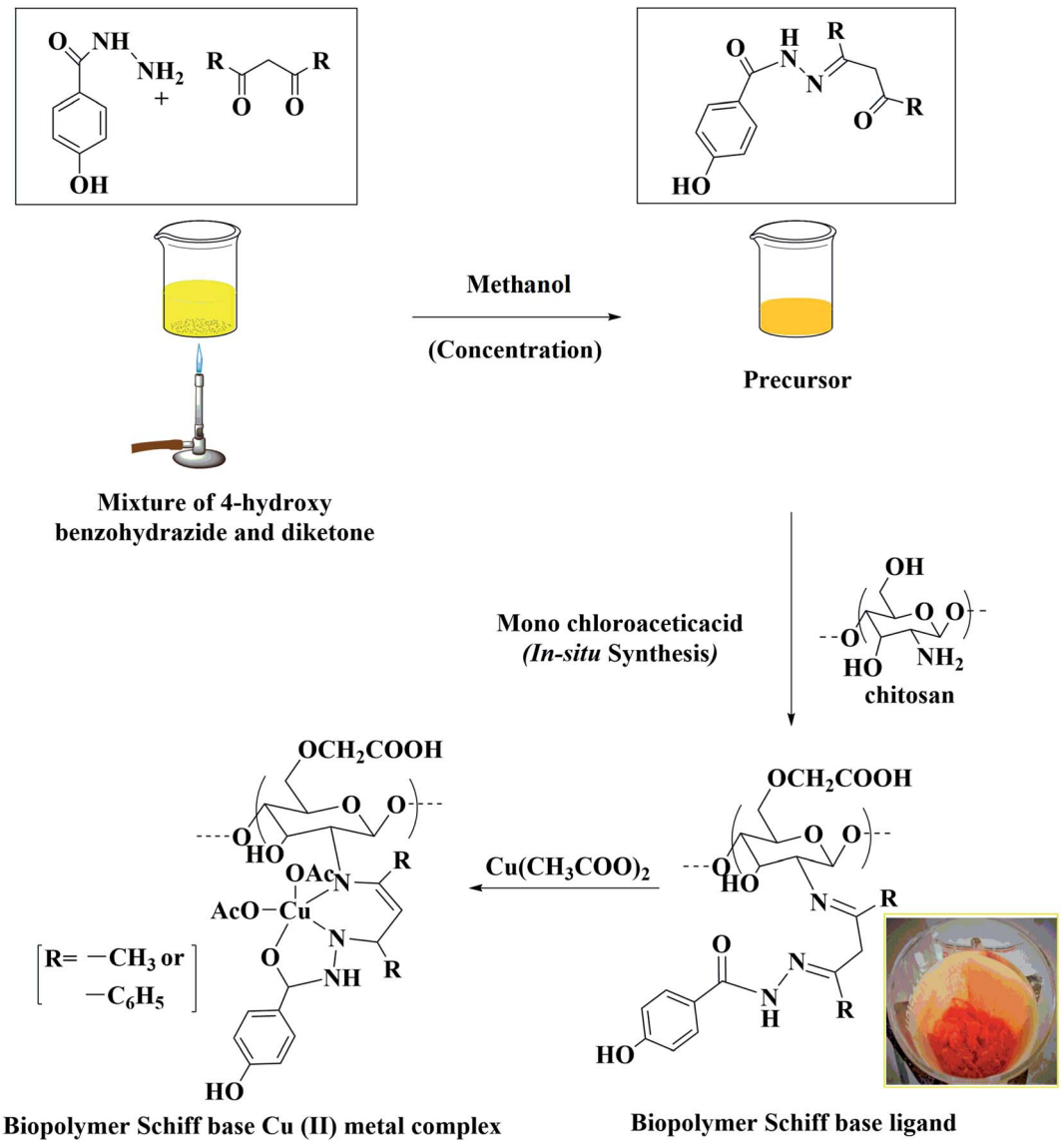

Scheme 1 Working design and synthesis of water soluble biopolymer/*O*-carboxymethyl chitosan Schiff bases and their Cu(II) complexes through an *in situ* synthesis.

standard drug acarbose at different doses of 10, 25, 50, 100 and 200 μM dissolved in antidiabetic reagent (20 mM sodium phosphate buffer (pH 6.9), containing 6 mM sodium chloride) and then, the mixture was incubated with and without α-amylase (0.5 mg mL^{-1}) at 25 °C for 10 min. Starch solution (1%) was added to all the test mixtures and incubation was continued at 25 °C for 30 min. Then, the colouring reagent dinitrosalicylic acid (DNS) was added to the mixture to stop enzymatic reaction and incubation continued for about 5 min in a water bath. Finally, all the test samples were allowed to cool to room temperature, followed by the addition of distilled water. The absorbance of the samples was measured at 540 nm using a UV-visible spectrophotometer. The percentage inhibition of α-amylase for the compounds was calculated using the following formula:

$$\text{Percentage of } \alpha\text{-amylase inhibition} = \left[\frac{1 - A_e}{A_c}\right] \times 100 \quad (6)$$

where A_c and A_e are the absorbance of the control and extract, respectively.

3.2 Experiment

3.2.1 Preparation of deacetylated chitosan (DCS). Deacetylated chitosan was prepared according to the procedure reported elsewhere.[78] The obtained deacetylated chitosan yield was 97%, which is shown in Table 1.

3.2.2 Preparation of water soluble biopolymer Schiff base ligands (Schiff base-1 (SB_1) and Schiff base-2 (SB_2)) through an *in situ* synthetic method. The water soluble biopolymer Schiff base ligands with [4-hydroxy benzohydrazide (1.0 g, 6.58 mmol), acetyl acetone (0.66 g, 6.58 mmol)] and [4-hydroxy benzohydrazide (0.67 g, 6.78 mmol), dibenzoyl methane (1.0 g, 6.78 mmol)] were represented as HBA and HBD, respectively. The compounds were prepared as follows.

About 50 mL of methanol was added to HBA (4-hydroxy benzohydrazide, acetyl acetone) and HBD (4-hydroxy benzohydrazide, dibenzoyl methane) precursor and the mixture was concentrated until it became straw-yellow. About 0.5 g of DCS was dissolved in 2% acetic acid (25 mL) followed by the addition of 20 mL of methanol in a round-bottom flask. The mixture was stirred well at 60 °C in an oil bath until it became uniform. Then, the initially concentrated precursor (HBA and HBD) was added slowly to the DCS mixture and stirred well for 30 min. After the stirring, a solution of 2.5 g of monochloroacetic acid in 15 mL of methanol was added dropwise to the mixture and it was stirred at 60 °C for 5 days for SB_1 and for 8 days for SB_2. The resulting Schiff base ligands [(SB_1): yellow orange and (SB_2): reddish brown] were cooled in a refrigerator. The products SB_1 and SB_2 were washed and filtered with hot methanol to remove the unreacted precursors HBA and HBD completely, respectively. Finally, they were dried in a hot air oven at 50 °C for 6 h (yield: 76% and 75%, respectively), as shown in Table 1.

3.5.3 Synthesis of Cu(II) complexes. Copper(II) complexes of SB_1 and SB_2 were synthesized as follows. About 0.3 g *O*-carboxymethyl chitosan Schiff base ligand (SB_1 and SB_2) was dissolved in 20 mL double distilled (2D) water in a separate vessel followed by the addition of 0.5 g of $Cu(CH_3COO)_2 \cdot H_2O$ in 20 mL of 2D water. The mixture was stirred in oil bath at 60 °C for 6 h, and then allowed to cool to room temperature (RT), and the resulting precipitates [[(SB_1)–$Cu(OAc)_2$: dark green] and [(SB_2)–$Cu(OAc)_2$: light green]) were washed and filtered with 2D water and dried at 50 °C for 6 h in a hot air oven (Scheme 1). The yields were 54% and 58% for [(SB_1)–$Cu(OAc)_2$] and [(SB_2)–$Cu(OAc)_2$], respectively, as shown in Table 1.

3.5.4 Preparation of buffer (pH = 3, 7 and 12) solutions. The acidic (pH = 3) buffer solution was prepared using a mixture of 1.8 mL of 0.1 M sodium acetate and 98.2 mL of 0.1 M acetic acid. About 0.12 g of sodium dihydrogen phosphate and 0.88 g of disodium hydrogen phosphate were dissolved in 100 mL of distilled water for the neutral buffer solution. The basic buffer solution was prepared using a mixture of 100 mL of 0.05 M disodium hydrogen phosphate and 53 mL of 0.1 M sodium hydroxide solution.[79,80]

4. Conclusion

Two novel 4-hydroxy benzohydrazide-grafted *O*-carboxymethyl chitosan Schiff base ligands and their Cu(II) complexes were synthesized. The degree of substitution of ligands SB_1 and SB_2 was found to be 46% and 48%, respectively. The FT-IR analysis and the proton (^1H) and carbon (^{13}C) NMR spectral studies confirmed the presence of the imine group (C=NH) and hydrazone (>C=N–NH–) coupling in the Schiff bases. The XRD studies revealed the amorphous form of the Cu(II) metal complexes, which were found to be more active than the ligands for pharmaceutical and biomedical applications. The SEM images of the ligands dramatically changed during the reaction, thus proving the successful formation of the complexes. The EDAX spectra of the complexes revealed the presence of C, N, O and Cu elements and confirmed the insertion of the metal in the complexes. The anti-inflammatory activity of 91.45 ± 3.1% for SB_1–C $(OAc)_2$ was better than that of SB_2–$Cu(OAc)_2$. In contrast, the antidiabetic activity of 93.13 ± 3.2% for SB_2–$Cu(OAc)_2$ proved to be better than that of acarbose. Furthermore, both complexes showed better photocatalytic dye degradation results than that of the reported compounds. The degradation of MB at different irradiation times with the catalyst showed that the optimum time was 90 min with 87.62% for SB_1–$Cu(OAc)_2$ and 69.03% for SB_2–$Cu(OAc)_2$. Different dosages of the catalysts showed the best degradation of MB with 20 mg of SB_2–$Cu(OAc)_2$ resulting in 92.38% degradation and 15 mg of SB_2–$Cu(OAc)_2$ exhibited 86.80% respectively. The catalysts in basic medium exhibited the best photocatalytic degradation of MB at pH = 12 of about 94.55% for SB_1–$Cu(OAc)_2$ and about 96.11% for SB_2–$Cu(OAc)_2$. Thus, these water soluble eco-friendly catalysts can be utilized in the preparation of organic biaryl compounds through C–C coupling reactions.

Conflicts of interest

There are no conflicts of interest

Acknowledgements

The authors are thankful to the PG and Research Department of Chemistry, Islamiah College (Autonomous), Vaniyambadi, Tamil Nadu, India for availing the needed laboratory and instrument facilities.

References

1 R. G. Saratale, G. D. Saratale, J. S. Chang and S. P. Govindwar, Bacterial decolorization and degradation of azo dyes: a review, *J. Taiwan Inst. Chem. Eng.*, 2011, **42**(1), 138–157, DOI: 10.1016/j.jtice.2010.06.006.

2 E. A. Abdelrahman and R. M. Hegazey, Facile Synthesis of HgO Nanoparticles Using Hydrothermal Method for Efficient Photocatalytic Degradation of Crystal Violet Dye Under UV and Sunlight Irradiation, *J. Inorg. Organomet. Polym. Mater.*, 2018, **29**, 346–358, DOI: 10.1007/s10904-018-1005-6.

3 A. Naz, S. Arun, S. S. Narvi, M. S. Alam, A. Singh, P. Bhartiya and P. K. Dutta, Cu(II)-carboxymethyl chitosan-silane schiff base complex grafted on nano silica: structural evolution, antibacterial performance and dye degradation ability, *Int. J. Biol. Macromol.*, 2018, **110**, 215–226, DOI: 10.1016/j.ijbiomac.2017.11.112.

4 V. K. Mourya and N. N. Inamdar, Chitosan-modifications and applications: opportunities galore, *React. Funct. Polym.*, 2008, **68**(6), 1013–1051, DOI: 10.1016/j.reactfunctpolym.2008.03.002.

5 G. Li, P. Song, K. Wang, Q. Xue, W. Sui and X. Kong, An amphiphilic chitosan derivative modified by deoxycholic acid: preparation, physicochemical characterization, and application, *J. Mater. Sci.*, 2015, **50**(6), 2634–2642, DOI: 10.1007/s10853-015-8852-0.

6 S. U. Islam and B. S. Butola, Recent advances in chitosan polysaccharide and its derivatives in antimicrobial modification of textile materials, *Int. J. Biol. Macromol.*, 2018, **121**, 905–912, DOI: 10.1016/j.ijbiomac.2018.10.102.

7 C. Yu, X. Kecen and Q. Xiaosai, Grafting Modification of Chitosan, *Biopolym. Grafting: Synth. Prop.*, 2018, 295–364, DOI: 10.1016/b978-0-323-48104-5.00007-x.

8 T. Baran, A new chitosan Schiff base supported Pd(II) complex for microwave-assisted synthesis of biaryls compounds, *J. Mol. Struct.*, 2017, **1141**, 535–541, DOI: 10.1016/j.molstruc.2017.03.122.

9 Y. Jia, L. Lu, M. Zhu, C. Yuan, S. Xing and X. Fu, A dioxidovanadium (V) complex of NNO-donor Schiff base as a selective inhibitor of protein tyrosine phosphatase 1B: synthesis, characterization, and biological activities, *Eur. J. Med. Chem.*, 2017, **128**, 287–292, DOI: 10.1016/j.ejmech.2017.02.003.

10 M.-R. Ke, J.-D. Huang and S.-M. Weng, Comparison between non-peripherally and peripherally tetra-substituted zinc(II) phthalocyanines as photosensitizers: synthesis, spectroscopic, photochemical and photobiological properties, *J. Photochem. Photobiol., A*, 2009, **201**(1), 23–31, DOI: 10.1016/j.jphotochem.2008.09.011.

11 Y. Chen, W. Lei, Y. Hou, C. Li, G. Jiang, B. Zhang and X. Wang, Fine control on the photochemical and photobiological properties of Ru(II) arene complexes, *Dalton Trans.*, 2015, **44**(16), 7347–7354, DOI: 10.1039/c5dt00939a.

12 L. Wang, S. Duan, P. Jin, H. She, J. Huang, Z. Lei and Q. Wang, Anchored Cu(II) tetra(4-carboxylphenyl)porphyrin to P25 (TiO_2) for efficient photocatalytic ability in CO_2 reduction, *Appl. Catal., B*, 2018, **239**, 599–608, DOI: 10.1016/j.apcatb.2018.08.007.

13 L. Wang, P. Jin, S. Duan, H. She, J. Huang and Q. Wang, In-situ incorporation of copper(II) porphyrin functionalized zirconium MOF and TiO_2 for efficient photocatalytic CO_2 reduction, *Sci. Bull.*, 2019, **64**, 926–933, DOI: 10.1016/j.scib.2019.05.012.

14 Q. Wang, Q. Ma, J. Lian, J. Zhong, F. Wang, J. Li and R. Wang, Bovine serum albumin modified ZnO to degrade organic dyes under ultraviolet light irradiation, *New J. Chem.*, 2016, **40**(6), 5604–5610, DOI: 10.1039/c5nj03061g.

15 S. Shinde and N. Sekar, Synthesis, spectroscopic characteristics, dyeing performance and TD-DFT study of quinolone based red emitting acid azo dyes, *Dyes Pigm.*, 2019, **168**, 12–27, DOI: 10.1016/j.dyepig.2019.04.028.

16 A. C. Nwanya, L. C. Razanamahandry, A. K. H. Bashir, C. O. Ikpo, S. C. Nwanya, S. Botha and M. Maaza, Industrial Textile Effluent Treatment and Antibacterial Effectiveness of Zea mays L. dry Husk Mediated Bio-synthesized Copper Oxide Nanoparticles, *J. Hazard. Mater.*, 2019, **375**, 281–289, DOI: 10.1016/j.jhazmat.2019.05.004.

17 P. Hemalatha, S. N. Karthick, K. V. Hemalatha, M. Yi, H.-J. Kim and M. Alagar, La-doped ZnO nanoflower as photocatalyst for methylene blue dye degradation under UV irradiation, *J. Mater. Sci.: Mater. Electron.*, 2015, **27**(3), 2367–2378, DOI: 10.1007/s10854-015-4034-8.

18 Y.-Y. Dong, S. Liu, Y.-J. Liu, L.-Y. Meng and M.-G. Ma, Ag@Fe_3O_4@cellulose nanocrystals nanocomposites: microwave-assisted hydrothermal synthesis, antimicrobial properties, and good adsorption of dye solution, *J. Mater. Sci.*, 2017, **52**(13), 8219–8230, DOI: 10.1007/s10853-017-1038-1.

19 R. Jiang, H. Zhu, G. Zeng, L. Xiao and Y. Guan, Synergy of adsorption and visible light photocatalysis to decolor methyl orange by activated carbon/nanosized CdS/chitosan composite, *J. Cent. South Univ. Technol.*, 2010, **17**(6), 1223–1229, DOI: 10.1007/s11771-010-0623-0.

20 H. Wang, Y. Wu, P. Wu, S. Chen, X. Guo, G. Meng and Z. Liu, Environmentally benign chitosan as reductant and supporter for synthesis of Ag/AgCl/chitosan composites by one-step and their photocatalytic degradation performance under visible-light irradiation, *Front. Mater. Sci.*, 2017, **11**(2), 130–138, DOI: 10.1007/s11706-017-0383-y.

21 S. Yu, J. Cui, H. Jiang, C. Zhong and J. Meng, Facile fabrication of functional chitosan microspheres and study on their effective cationic/anionic dyes removal from aqueous solution, *Int. J. Biol. Macromol.*, 2019, **134**, 830–837, DOI: 10.1016/j.ijbiomac.2019.04.208.

22 W. Wang, X. Jiang and K. Chen, Lanthanide-doped chitosan nanospheres as cell nuclei illuminator and fluorescent nonviral vector for plasmid DNA delivery, *Dalton Trans.*, 2012, **41**(2), 490–497, DOI: 10.1039/c1dt11200g.

23 A. Debrassi, A. F. Correa, T. Baccarin, N. Nedelko, A. Slawska-Waniewska, K. Sobczak and C. A. Rodrigues, Removal of cationic dyes from aqueous solutions using N-benzyl-O-carboxymethylchitosan magnetic nanoparticles, *Chem. Eng. J.*, 2012, **183**, 284–293, DOI: 10.1016/j.cej.2011.12.078.

24 Q.-A. Qurrat-ul-Ain, S. Khurshid, Z. Gul, J. Khatoon, M. R. Shah, I. Hamid and F. Aslam, Anionic azo dyes removal from water using amine-functionalized cobalt–iron oxide nanoparticles: a comparative time-dependent study and structural optimization towards the removal mechanism, *RSC Adv.*, 2020, **10**(2), 1021–1041, DOI: 10.1039/c9ra07686g.

25 C. Wei, C. Cheng, J. Zhao, S. Zheng, M. Hao and H. Pang, Assembling CdS mesoporous nanosheets into 3D hierarchitectures for effective photocatalytic performance, *Dalton Trans.*, 2014, **43**(15), 5687–5693, DOI: 10.1039/c3dt52947a.

26 R. El-Sharkawy and H. A. El-Ghamry, Multi-walled carbon nanotubes decorated with Cu(II) triazole Schiff base complex for adsorptive removal of synthetic dyes, *J. Mol. Liq.*, 2019, **282**, 515–526, DOI: 10.1016/j.molliq.2019.02.137.

27 A. A. Kulkarni and B. M. Bhanage, Ag@AgCl Nanomaterial Synthesis Using Sugar Cane Juice and Its Application in Degradation of Azo Dyes, *ACS Sustainable Chem. Eng.*, 2014, **2**(4), 1007–1013, DOI: 10.1021/sc4005668.

28 E. A. Abdelrahman, Synthesis of zeolite nanostructures from waste aluminium cans for efficient removal of malachite green dye from aqueous media, *J. Mol. Liq.*, 2018, **253**, 72–82, DOI: 10.1016/j.molliq.2018.01.038.

29 M. Y. Nassar and E. A. Abdelrahman, Hydrothermal tuning of the morphology and crystallite size of zeolite nanostructures for simultaneous adsorption and photocatalytic degradation of methylene blue dye, *J. Mol. Liq.*, 2017, **242**, 364–374, DOI: 10.1016/j.molliq.2017.07.033.

30 M. Y. Nassar, E. A. Abdelrahman, A. A. Aly and T. Y. Mohamed, A facile synthesis of mordenite zeolite nanostructures for efficient bleaching of crude soybean oil and removal of methylene blue dye from aqueous media, *J. Mol. Liq.*, 2017, **248**, 302–313, DOI: 10.1016/j.molliq.2017.10.061.

31 T. Basak, A. Bhattacharyya, K. Harms and S. Chattopadhyay, The ability of a trinuclear zinc(II) Schiff base complex to act as a photo catalyst for the degradation of methylene blue and to mimic phosphatase, *Polyhedron*, 2018, **157**, 449–457, DOI: 10.1016/j.poly.2018.09.070.

32 V. K. Bhardwaj, Potassium induced stitching of a flexible tripodal ligand into a bi-metallic two-dimensional coordination polymer for photo-degradation of organic dyes, *Dalton Trans.*, 2015, **44**(19), 8801–8804, DOI: 10.1039/c5dt01215e.

33 N. Hussain and V. K. Bhardwaj, The influence of different coordination environments on one-dimensional Cu(II) coordination polymers for the photo-degradation of organic dyes, *Dalton Trans.*, 2016, **45**(18), 7697–7707, DOI: 10.1039/c6dt00612d.

34 L.-J. Li, L.-K. Yang, Z.-K. Chen, Y.-Y. Huang, B. Fu and J.-L. Du, Synthesis and characterization of multifunctional Schiff base and Cu(II) complex: degradation of organic dyes and an optical property investigation, *Inorg. Chem. Commun.*, 2014, **50**, 62–64, DOI: 10.1016/j.inoche.2014.10.020.

35 G. Banuppriya, G. Shakambari, R. Sribalan, P. Varalakshmi and V. Padmini, Evaluation of Anticancer Activity of Water-Soluble Curcumin through the Induction of Apoptosis by p53 and p21 Modulation, *ChemistrySelect*, 2018, **3**(11), 2976–2981, DOI: 10.1002/slct.201800217.

36 W. Liu, Y. Qin, S. Liu, R. Xing, H. Yu, X. Chen and P. Li, Synthesis, characterization and antifungal efficacy of chitosan derivatives with triple quaternary ammonium groups, *Int. J. Biol. Macromol.*, 2018, **114**, 942–949, DOI: 10.1016/j.ijbiomac.2018.03.179.

37 Z. Jiang, Y. Song, J. Qiao, Y. Yang, W. Zhang, W. Liu and B. Han, Rat sciatic nerve regeneration across a 10-mm defect bridged by a chitin/CM-chitosan artificial nerve graft, *Int. J. Biol. Macromol.*, 2019, **129**, 997–1005, DOI: 10.1016/j.ijbiomac.2019.02.080.

38 H. Srinivasan, V. Kanayairam and R. Ravichandran, Chitin and chitosan preparation from shrimp shells Penaeus monodon and its human ovarian cancer cell line, PA-1, *Int. J. Biol. Macromol.*, 2018, **107**, 662–667, DOI: 10.1016/j.ijbiomac.2017.09.035.

39 Ö. Acet, T. Baran, D. Erdönmez, N. H. Aksoy, İ. Alacabey, A. Menteş and M. Odabaşi, O-carboxymethyl chitosan Schiff base complexes as affinity ligands for immobilized metal-ion affinity chromatography of lysozyme, *J. Chromatogr. A*, 2018, **1550**, 21–27, DOI: 10.1016/j.chroma.2018.03.022.

40 H. M. Aly, M. E. Moustafa and E. A. Abdelrahman, Synthesis of mordenite zeolite in absence of organic template, *Adv. Powder Technol.*, 2012, **23**(6), 757–760, DOI: 10.1016/j.apt.2011.10.003.

41 M. Kaya, Y. S. Cakmak, T. Baran, M. Asan-Ozusaglam, A. Mentes and K. O. Tozak, New chitin, chitosan, and O-carboxymethyl chitosan sources from resting eggs of Daphnia longispina (Crustacea); with physicochemical characterization, and antimicrobial and antioxidant activities, *Biotechnol. Bioprocess Eng.*, 2014, **19**(1), 58–69, DOI: 10.1007/s12257-013-0488-9.

42 M. Y. Nassar, H. M. Aly, E. A. Abdelrahman and M. E. Moustafa, Synthesis, characterization, and biological activity of some novel Schiff bases and their Co(II) and Ni(II) complexes: a new route for Co_3O_4 and NiO nanoparticles for photocatalytic degradation of methylene blue dye, *J. Mol. Struct.*, 2017, **1143**, 462–471, DOI: 10.1016/j.molstruc.2017.04.118.

43 S. Aslkhademi, N. Noshiranzadeh, M. S. Sadjadi, K. Mehrani and N. Farhadyar, Synthesis, crystal structure and investigation of the catalytic and spectroscopic properties of a Zn(II) complex with Coumarin-hydrazone ligand,

Polyhedron, 2018, **160**, 115–122, DOI: 10.1016/j.poly.2018.12.023.

44 M. Manimohan, S. Pugalmani and M. A. Sithique, Biologically active novel N, N, O donor tridentate water soluble hydrazide based O-carboxymethyl chitosan Schiff base Cu(II) metal complexes: synthesis and characterisation, *Int. J. Biol. Macromol.*, 2019, **136**, 738–754, DOI: 10.1016/j.ijbiomac.2019.06.115.

45 T. Baran, A. Menteş and H. Arslan, Synthesis and characterization of water soluble O-carboxymethyl chitosan Schiff bases and Cu(II) complexes, *Int. J. Biol. Macromol.*, 2015, **72**, 94–103, DOI: 10.1016/j.ijbiomac.2014.07.029.

46 Q. Song, Z. Zhang, J. Gao and C. Ding, Synthesis and property studies of N-carboxymethyl chitosan, *J. Appl. Polym. Sci.*, 2010, **119**(6), 3282–3285, DOI: 10.1002/app.32925.

47 S. T. Chew, K. M. Lo, S. K. Sinniah, K. S. Sim and K. W. Tan, Synthesis, characterization and biological evaluation of cationic hydrazone copper complexes with diverse diimine co-ligands, *RSC Adv.*, 2014, **4**(106), 61232–61247, DOI: 10.1039/c4ra11716f.

48 M. Y. Nassar, H. M. Aly, M. E. Moustafa and E. A. Abdelrahman, Synthesis, Characterization and Biological Activity of New 3-substitued-4-amino-5-hydrazino-1,2,4-triazole Schiff Bases and Their Cu(II) Complexes: A New Approach to CuO Nanoparticles for Photocatalytic Degradation of Methylene Blue Dye, *J. Inorg. Organomet. Polym. Mater.*, 2017, **27**(5), 1220–1233, DOI: 10.1007/s10904-017-0569-x.

49 T. Baran, E. Aciksoz and A. Menteş, Carboxymethyl chitosan Schiff base supported heterogeneous palladium(II) catalysts for Suzuki cross-coupling reaction, *J. Mol. Catal. A: Chem.*, 2015, **407**, 47–52, DOI: 10.1016/j.molcata.2015.06.008.

50 T. Baran and A. Menteş, Polymeric material prepared from Schiff base based on O-carboxymethyl chitosan and its Cu(II) and Pd(II) complexes, *J. Mol. Struct.*, 2016, **1115**, 220–227, DOI: 10.1016/j.molstruc.2016.03.015.

51 A. A. Alhwaige, H. Ishida and S. Qutubuddin, Poly(benzoxazine-f-chitosan) films: the role of aldehyde neighboring groups on chemical interaction of benzoxazine precursors with chitosan, *Carbohydr. Polym.*, 2019, **209**, 122–129, DOI: 10.1016/j.carbpol.2019.01.016.

52 E. L. De Araujo, H. F. G. Barbosa, E. R. Dockal and É. T. G. Cavalheiro, Synthesis, characterization and biological activity of Cu(II), Ni(II) and Zn(II) complexes of biopolymeric Schiff bases of salicylaldehydes and chitosan, *Int. J. Biol. Macromol.*, 2017, **95**, 168–176, DOI: 10.1016/j.ijbiomac.2016.10.109.

53 E. A. Abdelrahman and R. M. Hegazey, Exploitation of Egyptian insecticide cans in the fabrication of Si/Fe nanostructures and their chitosan polymer composites for the removal of Ni(II), Cu(II), and Zn(II) ions from aqueous solutions, *Composites, Part B*, 2019, **166**, 382–400, DOI: 10.1016/j.compositesb.2019.02.027.

54 T. Baran and A. Menteş, Cu(II) and Pd(II) complexes of water soluble O-carboxymethyl chitosan Schiff bases: synthesis, characterization, *Int. J. Biol. Macromol.*, 2015, **79**, 542–554, DOI: 10.1016/j.ijbiomac.2015.05.021.

55 F. S. Pereira, S. Lanfredi, E. R. P. González, D. L. da Silva Agostini, H. M. Gomes and R. dos Santos Medeiros, Thermal and morphological study of chitosan metal complexes, *J. Therm. Anal. Calorim.*, 2017, **129**(1), 291–301, DOI: 10.1007/s10973-017-6146-2.

56 H. M. Aly, M. E. Moustafa, M. Y. Nassar and E. A. Abdelrahman, Synthesis and characterization of novel Cu(II) complexes with 3-substituted-4-amino-5-mercapto-1,2,4-triazole Schiff bases: a new route to CuO nanoparticles, *J. Mol. Struct.*, 2015, **1086**, 223–231, DOI: 10.1016/j.molstruc.2015.01.017.

57 T. Baran and A. Menteş, Highly efficient Suzuki cross-coupling reaction of biomaterial supported catalyst derived from glyoxal and chitosan, *J. Organomet. Chem.*, 2016, **803**, 30–38, DOI: 10.1016/j.jorganchem.2015.12.011.

58 Z. Fan, Y. Qin, S. Liu, R. Xing, H. Yu, X. Chen and P. Li, Synthesis, characterization, and antifungal evaluation of diethoxyphosphoryl polyaminoethyl chitosan derivatives, *Carbohydr. Polym.*, 2018, **190**, 1–11, DOI: 10.1016/j.carbpol.2018.02.056.

59 T. Baran, A new chitosan Schiff base supported Pd(II) complex for microwave-assisted synthesis of biaryls compounds, *J. Mol. Struct.*, 2017, **1141**, 535–541, DOI: 10.1016/j.molstruc.2017.03.122.

60 E. A. Abdelrahmana, R. M. Hegazey and R. E. El-Azabawyc, Efficient removal of methylene blue dye from aqueous media using Fe/Si, Cr/Si, Ni/Si, and Zn/Si amorphous novel adsorbents, *J. Mater. Res. Technol.*, 2019, **8**(6), 5301–5313, DOI: 10.1016/j.jmrt.2019.08.051.

61 A. A. El-Asmy, A. Shabana, W. A. El-Maaty and M. M. Mostafa, Synthesis, spectroscopic characterization, molecular modeling and eukaryotic DNA degradation of new hydrazone complexes, *Arabian J. Chem.*, 2017, **10**, S936–S945, DOI: 10.1016/j.arabjc.2012.12.032.

62 N. A. Anan, S. M. Hassan, E. M. Saad, I. S. Butler and S. I. Mostafa, Preparation, characterization and pH-metric measurements of 4-hydroxysalicylidenechitosan Schiff-base complexes of Fe(III), Co(II), Ni(II), Cu(II), Zn(II), Ru(III), Rh(III), Pd(II) and Au(III), *Carbohydr. Res.*, 2011, **346**(6), 775–793, DOI: 10.1016/j.carres.2011.01.014.

63 S. A. Deodware, D. J. Sathe, P. B. Choudhari, T. N. Lokhande and S. H. Gaikwad, Development and molecular modeling of Co(II), Ni(II) and Cu(II) complexes as high acting anti breast cancer agents, *Arabian J. Chem.*, 2017, **10**(2), 262–272, DOI: 10.1016/j.arabjc.2016.09.024.

64 P. Singh, D. P. Singh, K. Tiwari, M. Mishra, A. K. Singh and V. P. Singh, Synthesis, structural investigations and corrosion inhibition studies on Mn(II), Co(II), Ni(II), Cu(II) and Zn(II) complexes with 2-amino-benzoic acid (phenyl-pyridin-2-yl-methylene)-hydrazide, *RSC Adv.*, 2015, **5**(56), 45217–45230, DOI: 10.1039/c4ra11929k.

65 E. Ispir, M. Ikiz, A. Inan, A. B. Sünbül, S. E. Tayhan, S. Bilgin and M. Elmastaş, Synthesis, Structural Characterization, Electrochemical, Photoluminescence, Antiproliferative and Antioxidant Properties of Co(II), Cu(II) and Zn(II) Complexes

Bearing the Azo-Azomethine Ligands, *J. Mol. Struct.*, 2019, **1182**, 63–71, DOI: 10.1016/j.molstruc.2019.01.029.

66 L.-L. Qian, Z.-X. Wang, L.-M. Zhu, K. Li, B.-L. Li and B. Wu, Synthesis, structure, spectral characteristic and photocatalytic degradation of organic dyes of a copper metal-organic framework based on tri(triazole) and pimelate, *Spectrochim. Acta, Part A*, 2019, **214**, 372–377, DOI: 10.1016/j.saa.2019.02.059.

67 M. S. Begum, E. Zangrando, M. B. H. Howlader, M. C. Sheikh, R. Miyatake, M. M. Hossain and M. A. Hasnat, Synthesis, characterization, photoluminescence and electrochemical studies of Ni II , Cu II , Zn II , Cd II and Pd II complexes of the bidentate S-hexyl-β-N-(2-thienyl)methylenedithiocarbazate ligand, *Polyhedron*, 2016, **105**, 56–61, DOI: 10.1016/j.poly.2015.11.046.

68 N. Nishat and A. Malik, Biodegradable coordination polymer: polycondensation of glutaraldehyde and starch in complex formation with transition metals Mn(II), Co(II), Ni(II), Cu(II) and Zn(II), *Arabian J. Chem.*, 2016, **9**, S1824–S1832, DOI: 10.1016/j.arabjc.2012.05.002.

69 R. S. Dariani, A. Esmaeili, A. Mortezaali and S. Dehghanpour, Photocatalytic reaction and degradation of methylene blue on TiO_2 nano-sized particles, *Optik*, 2016, **127**(18), 7143–7154, DOI: 10.1016/j.ijleo.2016.04.026.

70 N. B. Gopal Reddy, P. Murali Krishna and N. Kottam, Novel metal–organic photo catalysts: synthesis, characterization and decomposition of organic dyes, *Spectrochim. Acta, Part A*, 2015, **137**, 371–377, DOI: 10.1016/j.saa.2014.08.045.

71 S. Harish, M. Navaneethan, J. Archana, A. Silambarasan, S. Ponnusamy, C. Muthamizhchelvan and Y. Hayakawa, Controlled synthesis of organic ligand passivated ZnO nanostructures and their photocatalytic activity under visible light irradiation, *Dalton Trans.*, 2015, **44**(22), 10490–10498, DOI: 10.1039/c5dt01572c.

72 A. Naz, S. Arun, S. S. Narvi, M. S. Alam, A. Singh, P. Bhartiya and P. K. Dutta, Cu(II)-carboxymethyl chitosan-silane schiff base complex grafted on nano silica: structural evolution, antibacterial performance and dye degradation ability, *Int. J. Biol. Macromol.*, 2018, **110**, 215–226, DOI: 10.1016/j.ijbiomac.2017.11.112.

73 M. S. Aguilar and G. Rosas, A new synthesis of Cu_2O spherical particles for the degradation of methylene blue dye, *Environ. Nanotechnol. Monit. Manage.*, 2018, **11**, 100195, DOI: 10.1016/j.enmm.2018.100195.

74 L.-J. Li, L.-K. Yang, Z.-K. Chen, Y.-Y. Huang, B. Fu and J.-L. Du, Synthesis and characterization of multifunctional Schiff base and Cu(II) complex: degradation of organic dyes and an optical property investigation, *Inorg. Chem. Commun.*, 2014, **50**, 62–64, DOI: 10.1016/j.inoche.2014.10.020.

75 S. Farhadi, F. Mahmoudi, M. Dusek, V. Eigner and M. Kucerakova, A new inorganic–organic nanohybrid based on a copper(II) semicarbazone complex and the $PMo_{12}O_{40}^{3-}$ polyanion: synthesis, characterization, crystal structure and photocatalytic activity for degradation of cationic dyes, *Polyhedron*, 2017, **122**, 247–256, DOI: 10.1016/j.poly.2016.11.034.

76 J. Sheorain, M. Mehra, R. Thakur, S. Grewal and S. Kumari, In vitro anti-inflammatory and antioxidant potential of thymol loaded bipolymeric (tragacanth gum/chitosan) nanocarrier, *Int. J. Biol. Macromol.*, 2018, **125**, 1069–1074, DOI: 10.1016/j.ijbiomac.2018.12.095.

77 Y. Liu, S. Zeng, Y. Liu, W. Wu, Y. Shen, L. Zhang and C. Wang, Synthesis and antidiabetic activity of selenium nanoparticles in the presence of polysaccharides from Catathelasma ventricosum, *Int. J. Biol. Macromol.*, 2018, **114**, 632–639, DOI: 10.1016/j.ijbiomac.2018.03.161.

78 M. Murugaiyan, S. P. Mani and M. A. Sithique, Zinc(II) centered biologically active novel N, N, O donor tridentate water-soluble hydrazide-based O-carboxymethyl chitosan Schiff base metal complexes: synthesis and characterisation, *New J. Chem.*, 2019, **43**, 9540–9554, DOI: 10.1039/c9nj00670b.

79 R. J. Johnson, and D. E. Metzler, [1] Buffer preparation, *Enzyme Purification and Related Techniques*, 1971, vol. 22, pp. 3–5, DOI: 10.1016/0076-6879(71)22003-6.

80 G. Krohne, Lamins, *Methods in Cell Biology*, 2004, vol. 78, pp. 573–596. DOI: 10.1016/s0091-679x (04)78020-6.